AD_____

AWARD NUMBER: W81XWH-04-1-0870

TITLE: Optical Strategies for Studying Metastatic Mechanisms, Tumor Cell Detection and Treatment of Prostate Cancer

PRINCIPAL INVESTIGATOR: Nicolas Solban, Ph.D.

CONTRACTING ORGANIZATION: Massachusetts General Hospital
Boston, Massachusetts 02114-2554

REPORT DATE: October 2006

TYPE OF REPORT: Annual Summary

PREPARED FOR: U.S. Army Medical Research and Materiel Command
Fort Detrick, Maryland 21702-5012

REPORT DOCUMENTATION PAGE

Form Approved
OMB No. 0704-0188

1. REPORT DATE *(DD-MM-YYYY)*	**2. REPORT TYPE**	**3. DATES COVERED** *(From - To)*
01-10-2006	Annual Summary	15 Sep 2004 – 14 Sep 2006

4. TITLE AND SUBTITLE

Optical Strategies for Studying Metastatic Mechanisms, Tumor Cell Detection and Treatment of Prostate Cancer

5a. CONTRACT NUMBER

5b. GRANT NUMBER
W81XWH-04-1-0870

5c. PROGRAM ELEMENT NUMBER

6. AUTHOR(S)

Nicolas Solban, Ph.D.

E-Mail: nsolban@partners.org

5d. PROJECT NUMBER

5e. TASK NUMBER

5f. WORK UNIT NUMBER

7. PERFORMING ORGANIZATION NAME(S) AND ADDRESS(ES)

Massachusetts General Hospital
Boston, Massachusetts 02114-2554

8. PERFORMING ORGANIZATION REPORT NUMBER

9. SPONSORING / MONITORING AGENCY NAME(S) AND ADDRESS(ES)
U.S. Army Medical Research and Materiel Command
Fort Detrick, Maryland 21702-5012

10. SPONSOR/MONITOR'S ACRONYM(S)

11. SPONSOR/MONITOR'S REPORT NUMBER(S)

12. DISTRIBUTION / AVAILABILITY STATEMENT
Approved for Public Release; Distribution Unlimited

13. SUPPLEMENTARY NOTES

14. ABSTRACT

Prostate cancer is the most common cancer in men. Current treatments have limitations due to undesirable side effects. The objective of this proposal is to evaluate the effect of photodynamic therapy (PDT) on prostate tumors in order to design optimal treatment regimens. We have shown that subcurative PDT induces the release of the Vascular Endothelial Growth Factor (VEGF) both in vitro and in an orthotopic model of prostate cancer. Furthermore, we report that combining PDT with an antiangiogenic molecule, to prevent the action of VEGF,improves local control of prostate cancer and reduces the incidence of metastasis. Using a highly aggressive and metastatic prostate cancer cell line, we also report a PDT-induced decrease in β1 integrin coinciding with a decrease in adhesion to the extracellular matrix protein, collagen IV. Finally experimental metastasis assay showed that PDT-treated cells circulate longer in animals than control cells. We conclude that the most effective application of PDT for long-term cure, may involve combined therapeutic regimens.

15. SUBJECT TERMS
Cancer, Optical Imaging, Prostate, Metastasis, Treatment, Photodynamic Therapy, Biological Response

16. SECURITY CLASSIFICATION OF:			**17. LIMITATION OF ABSTRACT**	**18. NUMBER OF PAGES**	**19a. NAME OF RESPONSIBLE PERSON**
a. REPORT	**b. ABSTRACT**	**c. THIS PAGE**			USAMRMC
U	U	U	UU	91	**19b. TELEPHONE NUMBER** *(include area code)*

Table of Contents

Introduction

Prostate cancer is the most commonly diagnosed cancer, and associated mortality is only second to lung cancer. Current treatments for localized prostate cancer include: surgery (radical prostatectomy), androgen suppression hormone therapy, radiation therapy, cryotherapy, chemotherapy, and watchful waiting. Although current treatment modalities are only palliative for metastatic prostate cancer, they provide potential curative treatments for organ-confined prostate cancer. However, these treatments have limitations since significant complications, such as urinary incontinence, impotence, and rectal complications can arise due to the damage of the surrounding tissue. Therefore, any new treatment that can destroy prostate cancer cells without risking injury to the surrounding tissue would be highly desirable for localized prostate cancer. Photodynamic therapy (PDT) represents a promising alternative for the treatment of recurrent prostate cancer.
Numerous preclinical studies demonstrated the feasibility of using PDT for the treatment of prostate cancer. The transport of PS in the canine prostate (1, 2) or in the rat prostate (3) as been investigated optically and the irradiation of canine prostate showed significant necrosis with minimal damage to the surrounding tissues (4, 5) with careful dosimetry. Two small clinical trials confirmed the effectiveness and low incidence of complications associated with PDT treatment of human prostate cancer. Both studies reported minimal damage to surrounding tissue and the preservation of the anatomical feature of the prostate. In the first trial Windahl et al. (6) treated 2 patients with localized tumors following prostate resection and found that PDT significantly reduced levels of the Prostate Specific Antigen (PSA) and did not cause any severe complications. In the second trial, Nathan et al. (7) reported cancer necrosis and decrease PSA levels in recurrent prostate cancer following radiation therapy. Furthermore, this was associated with a lower incidence of complications than conventional treatment.
The objective of this proposal was to evaluate the effect of PDT on prostate tumors in order to design optimal treatment regimens. The primary hypothesis of this study is that PDT affects adhesion of prostate cancer cells to extracellular matrix proteins and induces Vascular Endothelial Growth Factor (VEGF) release. It is well established that VEGF can induce new vessel formation and vascular permeability. Together these events could lead to distant metastasis.

Body

The following section addresses the original statement of work by providing an up to date report of the progress.

Task 1: evaluation of the effect of PDT on prostate cancer cells.
a) In the current study we have used 2 prostate cancer cell lines. The LNCaP human prostate cancer cells initially isolated from a lymph node biopsy are useful for studying early stage of prostate cancer since they are androgen-dependant and have low metastatic potential. We have also used the MatLyLu (MLL) rat prostate cancer cells. These cells are useful for studying late stage prostate cancer since they are androgen independent and highly metastatic. Cells were incubated with [140 nM] of the photosensitizer BPD for 1 h, and then irradiated with a 690 nm laser at different light doses. 24 h following treatment cell viability was assayed using the standard MTT assay (Figure 1). Since this proposal is interested in the effect of subcurative PDT we have chosen the following light doses for LNCaP: 0.25 J/cm^2 and 0.5 J/cm^2, which correspond to 85% and 65% survival respectively (**Figure 1**, left) and 1 J/cm^2 and 3 J/cm^2 for MLL, which corresponds to 65% and 20% survival respectively (**Figure 1**, right).

b) We have used the conditions established in task 1(a) to test the adhesion of PDT treated MLL cells to the extracellular matrix protein collagen IV. MLL cells were treated with 140 nM BPD for 1 h and irradiated with 1 J/cm^2 and 3 J/cm^2. 24 h and 72 h following treatment cells were collected and plated on collagen IV plates and left to adhere for 4 h. % adhesion of cells was calculated by dividing the number

of cells after washing to the total number of cells plated. Following subcurative PDT, MLL cells have a decrease adhesion to collagen IV (**Figure 2**, left graph). At the higher light dose (3 J/cm^2) the adhesion is reduced to 15%. However this decrease is transient since after 72 h the adhesion is back to control level (**Figure 2**, right graph).

c) Subcurative PDT transiently decreases β1 integrin protein levels. The α5β1 integrin is highly expressed in MLL cells (8, 9) and mediates adhesion to collagen IV. We therefore, evaluated the levels of α5 and β1 integrin following PDT. Figure 3 shows representative western blot detecting β1 integrin and α5 integrin, together with actin as a loading control. PDT treatment with the higher light dose transiently decreases β1 integrin protein levels (Figure 3, A), 24 h after treatment. β1 integrin levels return to control levels 72 h after PDT Figure 3, B. Surprisingly, α5 integrin levels were not decreased following PDT. To elucidate the mechanism of this decrease, we measured RNA levels following treatment. Real-time PCR analysis did not show any decrease in mRNA transcript of either α5 integrin or β1 integrin (Figure 3, C and D respectively), suggesting a post-translational effect of PDT.

d) In the LNCaP cells, BPD is localized in the mitochondria and also in the cytosol (data not shown). This extra-mitochondrial localization suggests that PDT could also affect cytoplasmic molecules. The time course analysis of VEGF release at 8 h, 16 h, and 24 h following PDT with the two subcurative doses (determined in task a) is presented in **Figure 4**, A; results were normalized to cell number. Treatment with 0.25 J/cm2 and 0.5 J/cm2 led to a 1.6-fold and to a 2.1-fold increase ($p<0.01$, **Figure 4**, A) in VEGF respectively when compared to light only (LO) or to BPD only (BO) 24 h after treatment. Viability assay showed that cell death following BPD-PDT occurs before 8 h and that the number of cells for each group does not significantly vary between 8 h and 24 h (data not shown). Furthermore, since there is no increase in VEGF after 8 h or 16 h (**Figure 4**, A), this suggests that the observed increase in VEGF following PDT is not due to the release of intracellular VEGF from dead cells.
To determine the mechanism of this increase, PDT-treated LNCaP cells were collected 24 h following treatment, and intracellular VEGF levels were measured by ELISA. The results were normalized to protein concentration (**Figure 4**, B). A significant increase ($p<0.05$) in intracellular VEGF at 0.5 J/cm^2 (1.4-fold) was observed (**Figure 4**, B). Surprisingly, despite an increase of VEGF in the cell-conditioned media after the lower dose treatment (0.25 J/cm^2), there was no significant increase in the intracellular VEGF protein levels. In order to establish the mechanism of this increase, we used primers specific for exon 1 and exon 8 of the VEGF gene to determine VEGF mRNA levels following PDT. As previously described (10), these primers can amplify all possible isoforms of VEGF. **Figure 4**, C shows a representative picture of an RT-PCR experiment following PDT. Only 3 isoforms of VEGF are expressed in LNCaP cells: $VEGF_{121}$, $VEGF_{145}$, and $VEGF_{165}$, with $VEGF_{121}$ being the most abundant and $VEGF_{145}$ being the least abundant. With the 0.5 J/cm^2 treatment, all 3 VEGF isoforms are increased (**Figure 4**, C). **Figure 4**, D shows the average fold induction of each VEGF isoform following GAPDH normalization. All 3 isoforms detected are increased, but only following the 0.5 J/cm^2 PDT treatment. Concordant with intracellular protein levels, there is a significant ($p<0.001$) increase in mRNA levels of $VEGF_{121}$, $VEGF_{145}$, and $VEGF_{165}$ (1.5-fold, 1.5-fold, and 1.6-fold increase respectively when compared to no treatment). However, since it is known that VEGF can be regulated both at the transcriptional (11, 12)and at the post-transcriptional levels (12-14), from these experiments we cannot exclude either mechanism.

Task 2: Design of optical monitoring tools to detect circulating prostate cancer cells.
a) Since the Prostate Specific Membrane Antigen (PSMA) is expressed almost exclusively on prostate cancer cells it is a reliable marker for the detection of circulating prostate cancer cells. We have tested the expression of PSMA in LNCaP and MLL cells by western analysis. Figure 5 shows that the Ab used detects PSMA only in LNCaP cells both *in vitro* and *in vivo*. Furthermore PDT treatment of LNCaP

tumors does not affect PSMA expression. On the other hand PSMA cannot be detected in MLL cells *in vitro* or *in vivo* using this Ab. Therefore our PSMA Ab cannot be used to detect circulating MLL cells. Other methods for detecting these cells are currently under investigation.

b) We have labeled PSMA Ab with the fluorescent dye Cy5.5, or Cy5. The free dye was separated from conjugated antibody using a gel filtration column. Using this conjugation method we obtained a dye/antibody ratio of about 3 and a recovery of about 90%. To confirm that labeled PSMA maintained its specificity we have incubated LNCaP cells and MLL cells with 5 μg of labeled PSMA-Cy5.5 for 15 min at 37^{o}C. Similar to western blot results, Figure 6 shows that only LNCaP cells are labeled by PSMA, confirming that PSMA-Cy5.5 maintained its specificity.

c) LNCaP cells were labeled with PSMA-Cy5.5, PSMA- Cy5, or with PSMA-Qdots. Fluorescence was measured by FACS. As shown in Figure 7, LNCaP cells labeled with PSMA-Qdots are about 10x brighter than LNCaP cells labeled with PSMA-Cy5. We were not able to detect LNCaP cells labeled with PSMA-Cy5.5 since the instrument doesn't have the proper filters. These cells were then injected in the tail vain of SCID mice and the animals were placed on the *in vivo* cytometer to detect circulating cells (15). We were not able to detect cells labeled with PSMA-Cy5 or cells labeled with PSMA-Cy5.5. However we were able to count cells labeled with PSMA-Qdots. Therefore for task 3 we will use PSMA-Qdots to detect circulating prostate cancer cells.

d) LNCaP and MLL cells were stably transfected with the plasmid pEGFP-N1 (Clontech). This plasmid codes for the green fluorescent protein (GFP). Stable cells were established after selection in the antibiotic G418. A heterogeneous population of cells of different fluorescence intensity is obtained after transfection (Figure 8). The highly fluorescent population of cells (M1 in Figure 8) was sorted by FACS and used for future experiments.

e) Stably tranfected GFP cells were injected in the tail vein of animals and the *in vivo* cytometer was used to detect them. However, we were not able to detect these cells even though they are very fluorescent. This is most likely due to the absorption of green fluorescence by blood. In order to detect circulating cancer cells we will use antibodies labeled with Qdots since we have shown in task II (c) that these labeled cells are highly fluorescent and can easily be detected using the *in vivo* flow cytometer.

Task 3: Evaluation of cells shedding following PDT treatment.
a) *Subcurative PDT increases circulation time of MLL cells.* Adhesion molecules are required for homing of circulating cancer cells and subcurative PDT-treatment decreases adhesion to collagen IV. Therefore, we evaluated the effect of subcurative PDT on the circulation time of MLL cells. PDT-treated or untreated MLL cells were labeled with the lipophilic fluorescent dye, DiD, prior to intravenous injection in animals. Live, anesthetized animals were placed on the IVFC to count circulating cells (15). Untreated cells are very rapidly cleared from circulation, 30 min after injection, there is a ~ 80 % decrease in the number of circulating cells (Figure 9, gray plot). However, when cells are injected 24 h following PDT, there is a significant ($P < 0.05$ when compared to control) increase in circulation time (Figure 9, dash plot), while cells injected 72 h post-PDT have similar circulation time than control (Figure 9, black plot).

Task 4: Biological effect of PDT on orthotopic prostate tumors.
a) In vivo decrease in β1 integrin following subcurative PDT. Orthotopic implantation of MLL cells is a well-established model of androgen-independent prostate cancer. This cell line is fast growing, poorly differentiated, and metastatic to the lungs and lymph nodes. To determine if this subcurative PDT-induced decrease in β1 integrin also occurred in vivo, we implanted MLL cells in the prostate of

Copenhagen rats and treated them with 50 J/cm^2. The PDT regimen used has previously been demonstrated to be subcurative (16). Twenty-four hours following treatment, animals were euthanized and the prostate was collected and fixed in 10 % formalin. Figure 10 show immunohistochemical staining using β1 integrin Ab. Similar to in vitro results; there is a decrease in β1 integrin protein levels following PDT treatment. Figure 10, right panels, arrow, shows an area unaffected by PDT treatment. This area probably did not receive enough light or PS, or both to elicit visible damage. Proteins were also extracted from PDT treated tumors and western blot analysis was performed to determine the levels of α5 and β1 integrin. There is a significant decrease in β1 protein levels (Figure 11, left picture) following PDT, however there is no decrease in α5 integrin protein levels (Figure 11, right picture). The average densitometric quantification from 5 different animals is presented in the lower bar graph after taking the ratio integrin: actin. Following PDT there is a 5-fold decrease in β1 integrin protein levels (Figure 11, left bar graph); but no significant decrease in α5 integrin protein levels. From the same PDT-treated tumors RNA was extracted, there is a significant decrease in β1 integrin mRNA levels following treatment ($P < 0.001$ when compared to no treatment) and, surprisingly, a significant increase in α5 integrin mRNA ($P < 0.05$ when compared to no treatment, Figure 11, C and D).

b) *In vivo effects of PDT*. To study the *in vivo* effect of subcurative PDT, we have used an orthotopic prostate cancer model which was shown to more reliably mimic pathological conditions than ectopic models (17-19). Three weeks after LNCaP injection, a 0.1~0.2 cm^3 tumor will develop in 90% of cases. For *in vivo* studies we have used the FDA approved liposomal formulation of BPD (verteporfin®) since tumor accumulation was shown to be increased *in vivo* when compared to its non-liposomal formulation (20). For subcurative treatment, light was delivered with a fluence rate of 100 mW/cm^2 and a total fluence of 50 J/cm^2. This treatment was shown to be subcurative, but still causes significant tumor damage (data not shown). Therefore, it is ideal for the study of the response of tumors that have been exposed to both PS and light, but not at sufficient levels to kill them. Immunohistochemical analysis of tumors collected 24 h after treatment showed a more intense VEGF staining following PDT treatment (**Figure 12**, bottom images, compare C to A and to B). **Figure 12** (top) images show the hematoxylin and eosin staining of tumor sections. There were numerous necrotic areas observed after PDT treatment (**Figure 12** C top, arrows) and a significant infiltration of red blood cells indicative of effective treatment. To have a more quantitative approximation of the VEGF increase, we collected proteins from tumors 24 h after treatment. VEGF ELISA was performed and all results were normalized to protein concentration. This ELISA not only detects intracellular VEGF, but also cell/extracellular associated VEGF. There was a significant ($p<0.05$) increase in VEGF levels following PDT treatment (1.9-fold increase when compared to BPD only) in orthotopic prostate tumors (**Figure 13**), consistent with the immunohistochemical observations.

c) *Increased treatment efficacy when combining antiangiogenic therapy with PDT.* It is well documented that VEGF is a potent angiogenic molecule (21, 22). Therefore, the measured increase in VEGF following PDT could reduce treatment efficacy by promoting tumor regrowth or potentially facilitating metastasis. For these reasons we decided to investigate the efficacy of combining the antiangiogenic molecule, TNP-470, with PDT. **Figure 14** shows the various groups used in this study. Group D received TNP-470 every 2 days the week preceding PDT, while group E received TNP-470 every 2 days for the week following PDT. All animals were sacrificed 40 days following orthotopic implantation and the prostate, comprised of tumor tissue and normal tissue, was collected. Prostate weight and prostate volume were also significantly reduced ($P < 0.05$) in the PDT + TNP-470 group when compared to the control group (**Figure 15**, A). We did not measure any significant differences when TNP-470 was administered prior to PDT. It is important to note that, in the current study, we used subcurative PDT doses therefore the tumors at day 40 are > 400 mg compared to ~ 20 mg for normal prostate.

PDT increases the fraction of animals with lymph node metastases. At the time of sacrifice the lungs, pelvic lymph nodes, liver and spines were collected and metastatic spread was assessed. No metastases could be detected in the liver, spines and lungs in all groups. On the other hand, lymph node metastases were detected in some animals of every group. **Figure 15**, B shows the percentage of animals with lymph node metastases for each group. Similar to our previous report (16), more animals from group B (72%), which received only PDT, had metastases when compared to all other groups. Interestingly, the fraction of animals with lymph node metastases was reduced in all TNP-470-treated groups.

d) 2 published manuscripts and one submitted manuscript are appended.

Key Research Accomplishments

Travel Award:
1. 2005, European Society for Photobiology: Postdoctoral Fellow Travel Award.
2. 2004, American Society for Photobiology: Postdoctoral Fellow Travel Award.

Original Articles

1. **Solban Nicolas**, Georgakoudi Irene, Sung K Chang, Rice L William, Charles Lin, Hasan Tayyaba. Decrease adhesion to extracellular matrix following subcurative photodynamic therapy. *Submitted to Cancer Res.*

2. Kosharskyy Boleslav[*], **Solban Nicolas**[*], Chang K Sung, Rizvi Imran, Chang Yuchiao, Hasan Tayyaba. Antiangiogenic Therapy with Photodynamic Therapy: A mechanism-based combination that inhibits tumor growth and metastasis in an orthotopic model of prostate cancer. *Accepted for publication, in press.* (*Joint first authors).

3. **Solban Nicolas**, Selbo K Pål, Sinha K Alok, Chang K Sung, Hasan Tayyaba. Mechanistic Investigation and Implications of PDT-Induction of VEGF in Prostate Cancer. Cancer Res. 2006 May 15: 66(15):1-8.

4. **Solban N**, Rizvi R, Hasan T. Targeted Photodynamic Therapy. Lasers Surg Med. 2006 Jun;38(5):522-31.

5. Chen B, Pogue BW, Zhou X, O'Hara JA, **Solban N**, Demidenko E, Hoopes PJ, Hasan T. Effect of tumor host microenvironment on photodynamic therapy in a rat prostate tumor model. Clin Cancer Res. 2005 Jan 15;11(2 Pt 1):720-7.

Selected Full Proceedings of Meetings

1. **Nicolas Solban**, Irene Georgakoudi, William L. Rice, Charles Lin, Tayyaba Hasan. Role of cell type and animal species in tumor metastasis. In: David Kessel; Editor. Optical Methods for Tumor Treatment and Detection: Mechanisms and Techniques in Photodynamic Therapy XIII. Photonics West 2004. 2004 Jan 24-29; San Jose, USA. Proc. SPIE Vol. 5315, p 41-48

2. **Nicolas Solban**, Irene Georgakoudi, Bernhard Ortel and Charles Lin, Tayaaba Hasan. Optical imaging in photodynamic therapy: mechanisms and applications. In: Alexander P. Savitsky, Lubov Y. Brovko, Darryl J. Bornhop, Ramesh Raghavachari, Samuel I. Achilefu; Editors. Genetically Engineered and Optical Probes for Biomedical Applications II. Photonics West 2004. 2004 Jan 24-29; San Jose, USA. Proc. SPIE Vol. 5329, p. 192-200.

3. Tayyaba Hasan, **Nicolas Solban**. Photochemical Effects in Laser-tissue interactions: photodynamic therapy, an overview. In: Steven L. Jacques, William P. Roach; Editors. Laser Interaction with Tissue and Cells XV. Photonics West 2004. 2004 Jan 24-29; San Jose, USA. Proc. SPIE Vol: 5319, p. 41-49

4. **Nicolas Solban**, Nathaniel Sznycer-Taub, Juan Manuel Benavides, Sung Chang, Irene Georgakoudi, Tayyaba Hasan. The need for optical imaging in the understanding and optimization of photodynamic therapy. In: Darryl J. Bornhop, Samuel I. Achilefu, Ramesh Raghavachari, Alexander P. Savitsky; Editors. Genetically Engineered and Optical Probes for Biomedical Applications III. Proc. SPIE Vol: 5704, p. 1-9.

Book Chapters

1. Hasan T, Ortel B, **Solban N**, Moor CE, Pogue B. Photodynamic therapy of cancer. In: D.W. Kufe and R.R Weichselbaum, editors. Cancer Medicine. BC Decker Inc, 2005. Chapter 35a.

2. **Solban N**, Ortel B, Pogue B, **Hasan, T.** Targeted Optical Imaging and Photodynamic Therapy. In: A.A. Jr. Bogdanov and K Licha, editors. Molecular Imaging: An Essential Tool in Preclinical Research, Diagnostic Imaging, and Therapy. Heidelberg: Springer-Verlag, 2005: Chapter 12, 229-58.

3. **Solban N**, Ortel B, Pogue B, Hasan T. Targeted optical imaging and photodynamic therapy. In: Ernst Schering Res Found Workshop. 2005;(49):229-58.

Abstract:

1. I. Georgakoudi, **N. Solban**, C. Lin, T. Hasan. In vivo flow cytometry: A noninvasive method for monitoring circulating cells after PDT. *SPIE Optics East 2005*, Boston, MA, USA, 2005.

2. **N Solban,** I Georgakoudi, W. Rice, C Lin, T Hasan. Decrease in adhesion of prostate cancer cells following subcurative photodynamic therapy. *11th Congress of the European Society for Photobiology*. Aix-les-Bains, France, 2005.

3. **N Solban**, A Sinha, S Chang, W Rice, P K Selbo, T Hasan. Effect of photodynamic therapy on human prostate tumor microcirculation: potential mechanism of distant metastasis. *96th Annual meeting of the American Association for Cancer Research*, Anaheim, CA, USA, 2005

4. **N Solban**, W Rice, I Georgakoudi, N Sznycer-Taub, J Benavides, B Johnson, C Lin, T Hasan. Effect of Photodynamic Therapy on Prostate Cancer. *Tumor Progression and Therapeutic Resistance*, Philadelphia, PA, USA, 2004

5. **N Solban**, I Georgakoudi, W Rice, A Sinha, P K Selbo, C Lin, T Hasan. Molecular Responses of prostate cancer to photodynamic therapy and in vivo imaging of circulating prostate cancer cells. *American Society for Photobiology*, Seattle, WA USA, 2004.

Conclusions

PDT is an approved therapeutic modality for various oncologic and non-oncologic pathologies. This proposal studied the molecular responses of prostate cancer cells to various PDT treatment conditions in order to optimize treatment efficacy and minimize side effects. The results obtained establish that PDT alters cellular-molecular processes such as cell adhesion, as well as transcription and synthesis of VEGF in vivo and in vitro at subcurative doses. We also report that combining PDT with an antiangiogenic agent, to prevent the action of the PDT-induced VEGF secretion improves local control of prostate

cancer and reduces the incidences of metastasis. We conclude that the most effective application of PDT for long-term cure, may involve combined therapeutic regimens.

References

1. Zhu TC, Hahn SM, Kapatkin AS, et al. In vivo optical properties of normal canine prostate at 732 nm using motexafin lutetium-mediated photodynamic therapy. Photochem Photobiol 2003;77:81-8.

2. Solonenko M, Cheung R, Busch TM, et al. In vivo reflectance measurement of optical properties, blood oxygenation and motexafin lutetium uptake in canine large bowels, kidneys and prostates. Phys Med Biol 2002;47:857-73.

3. Hamblin MR, Rajadhyaksha M, Momma T, Soukos NS, Hasan T. In vivo fluorescence imaging of the transport of charged chlorin e6 conjugates in a rat orthotopic prostate tumour. Br J Cancer 1999;81:261-8.

4. Chen Q, Huang Z, Luck D, et al. Preclinical studies in normal canine prostate of a novel palladium-bacteriopheophorbide (WST09) photosensitizer for photodynamic therapy of prostate cancers. Photochem Photobiol 2002;76:438-45.

5. Hsi RA, Kapatkin A, Strandberg J, et al. Photodynamic therapy in the canine prostate using motexafin lutetium. Clin Cancer Res 2001;7:651-60.

6. Windahl T, Andersson SO, Lofgren L. Photodynamic therapy of localised prostatic cancer. Lancet 1990;336:1139.

7. Nathan TR, Whitelaw DE, Chang SC, et al. Photodynamic therapy for prostate cancer recurrence after radiotherapy: A phase I study. J Urol 2002;168:1427-32.

8. Livant DL, Brabec RK, Pienta KJ, et al. Anti-invasive, antitumorigenic, and antimetastatic activities of the PHSCN sequence in prostate carcinoma. Cancer Res 2000;60:309-20.

9. MacCalman CD, Brodt P, Doublet JD, et al. The loss of E-cadherin mRNA transcripts in rat prostatic tumors is accompanied by increased expression of mRNA transcripts encoding fibronectin and its receptor. Clin Exp Metastasis 1994;12:101-7.

10. Uthoff SM, Duchrow M, Schmidt MH, et al. VEGF isoforms and mutations in human colorectal cancer. Int J Cancer 2002;101:32-6.

11. Pages G, Pouyssegur J. Transcriptional regulation of the vascular endothelial growth factor gene--a concert of activating factors. Cardiovasc Res 2005;65:564-73.

12. Mukhopadhyay D, Datta K. Multiple regulatory pathways of vascular permeability factor/vascular endothelial growth factor (VPF/VEGF) expression in tumors. Semin Cancer Biol 2004;14:123-30.

13. Pages G, Berra E, Milanini J, Levy AP, Pouyssegur J. Stress-activated protein kinases (JNK and p38/HOG) are essential for vascular endothelial growth factor mRNA stability. J Biol Chem 2000;275:26484-91.

14. Liu LX, Lu H, Luo Y, et al. Stabilization of vascular endothelial growth factor mRNA by hypoxia-inducible factor 1. Biochem Biophys Res Commun 2002;291:908-14.

15. Georgakoudi I, Solban N, Novak J, et al. In vivo flow cytometry: A new method for enumerating circulating cancer cells. Cancer Res 2004;64:5044-7.

16. Momma T, Hamblin MR, Wu HC, Hasan T. Photodynamic therapy of orthotopic prostate cancer with benzoporphyrin derivative: Local control and distant metastasis. Cancer Res 1998;58:5425-31.

17. Chen B, Pogue BW, Zhou X, et al. Effect of tumor host microenvironment on photodynamic therapy in a rat prostate tumor model. Clin Cancer Res 2005;11:720-7.

18. Fukumura D, Yuan F, Monsky WL, Chen Y, Jain RK. Effect of host microenvironment on the microcirculation of human colon adenocarcinoma. Am J Pathol 1997;151:679-88.

19. Monsky WL, Mouta Carreira C, Tsuzuki Y, Gohongi T, Fukumura D, Jain RK. Role of host microenvironment in angiogenesis and microvascular functions in human breast cancer xenografts: Mammary fat pad versus cranial tumors. Clin Cancer Res 2002;8:1008-13.

20. Hasan T, Ortel B, Solban N, Pogue B. Photodynamic therapy of cancer. In: Kufe, Bast, Hait, Hong, Pollock, Weichselbaum, et al, editors. Cancer Medicine, 7th edition. Hamilton, Ontario: B.C. Decker, Inc; 2006. p. 537-548.

21. Hrouda D, Nicol DL, Gardiner RA. The role of angiogenesis in prostate development and the pathogenesis of prostate cancer. Urol Res 2003;30:347-55.

22. Nicholson B, Theodorescu D. Angiogenesis and prostate cancer tumor growth. J Cell Biochem 2004;91:125-50.

APPENDICES

Figure 1: Prostate cancer cell lines killing curve. LNCaP cells (left) or MLL cells (right) were incubated with BPD for 1 h and irradiated with different light doses. 24 h post-PDT viability was assayed. Grey bars show the light doses used in the subsequent experiments.

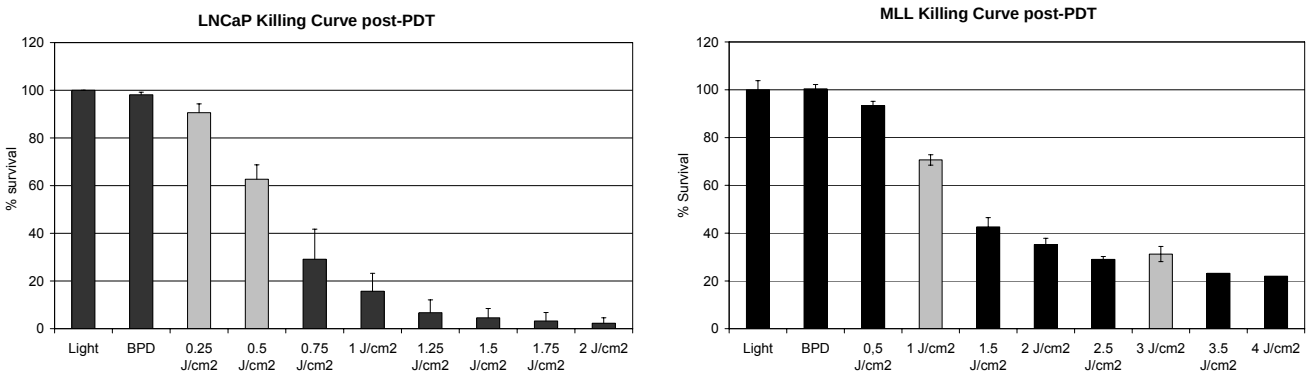

Figure 2: Transient decrease in adhesion following PDT. 24 h (left) and 72 h (right) after PDT MLL cells were collected and left to adhere for 4 h to collagen IV. % Adhesion was calculated by dividing the number of cells after washing to the total number of cells plated.

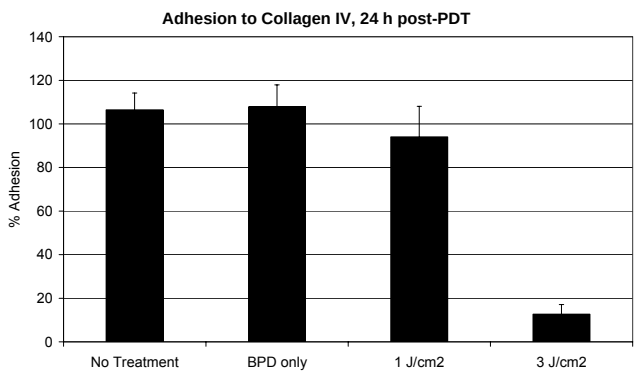

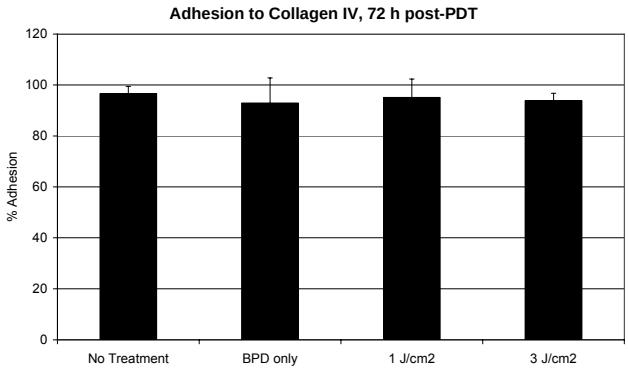

Figure 3: Decrease in Integrin β1 levels by subcurative PDT. 24 h following treatment (A) and 72 h following treatment (B) PDT treated cells were collected, protein was extracted and β1-Integrin or α5-integrin western analysis was performed. There is a transient decrease in Integrin β1 levels after 24 h (A) but the levels return to normal 72 h after treatment (B). However there's no decrease in α5-integrin following PDT. LO: light only, BO: BPD only. Actin was used as a loading control. Real-time RT-PCR analysis of α5-integrin (C) and β1 integrin (D) mRNA levels. Results are expressed relative to LO and are mean ± SE of 3 independent experiments measured in triplicate.

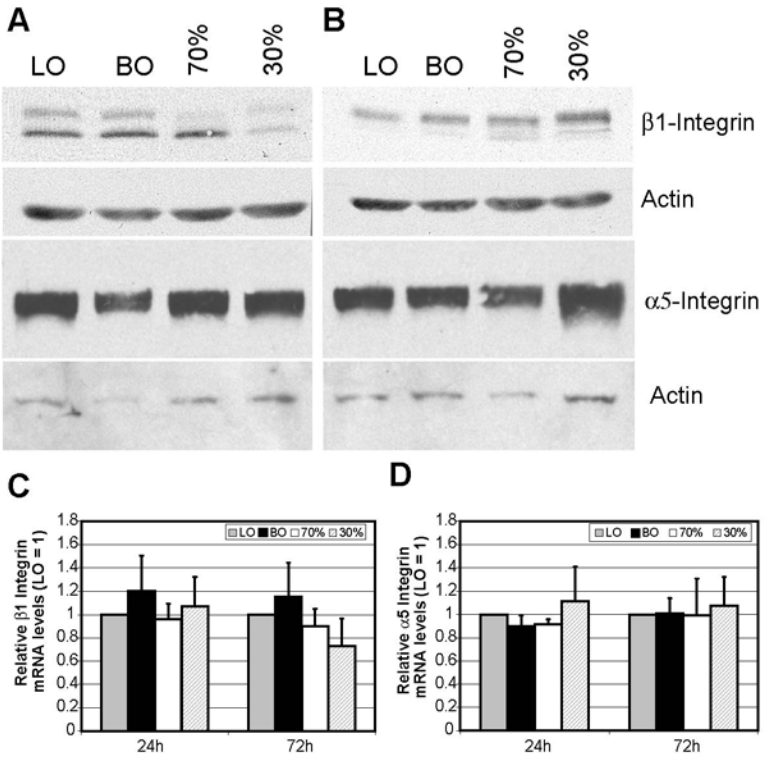

Figure 4: Increase of released and intracellular VEGF protein and mRNA following PDT. A) Time course analysis of PDT induced VEGF release. At 8 h, 16 h, and 24 h post PDT treatment, secreted VEGF was measured by ELISA in the cell medium. Values are normalized relative to cell number. A statistically significant increase in secreted VEGF is measured 24 h post-PDT (* $P < 0.01$ when compared to LO or to BO). (B) 24 h post PDT treatment intracellular VEGF was measured by ELISA and a statistically significant increase was measured only with the 0.5 J/cm2 light dose (* $P < 0.05$ when compared to NT, LO or to BO). Values are normalized relative to protein concentration. C) Representative agarose gel analyzing RT-PCR products for VEGF (517, 580, and 649 bp corresponding, respectively, to the 121, 145, and 165 protein isoforms, top gel) or GAPDH (bottom gel). All VEGF isoforms are increased following 0.5 J/cm2 treatment. D) The relative levels of VEGF were determined by RT-PCR analysis. The results are expressed as fold induction of VEGF mRNA after calculating VEGF: GAPDH ratio. There is a statistically significant ~1.5 fold induction in all VEGF isoforms following 0.5 J/cm2 treatment (* $P < 0.01$ when compared to NT, LO or to BO). NT was arbitrarily set at 1. NT: no treatment, LO: light only, BO: BPD only. Data represents the mean ± SE of three independent experiments.

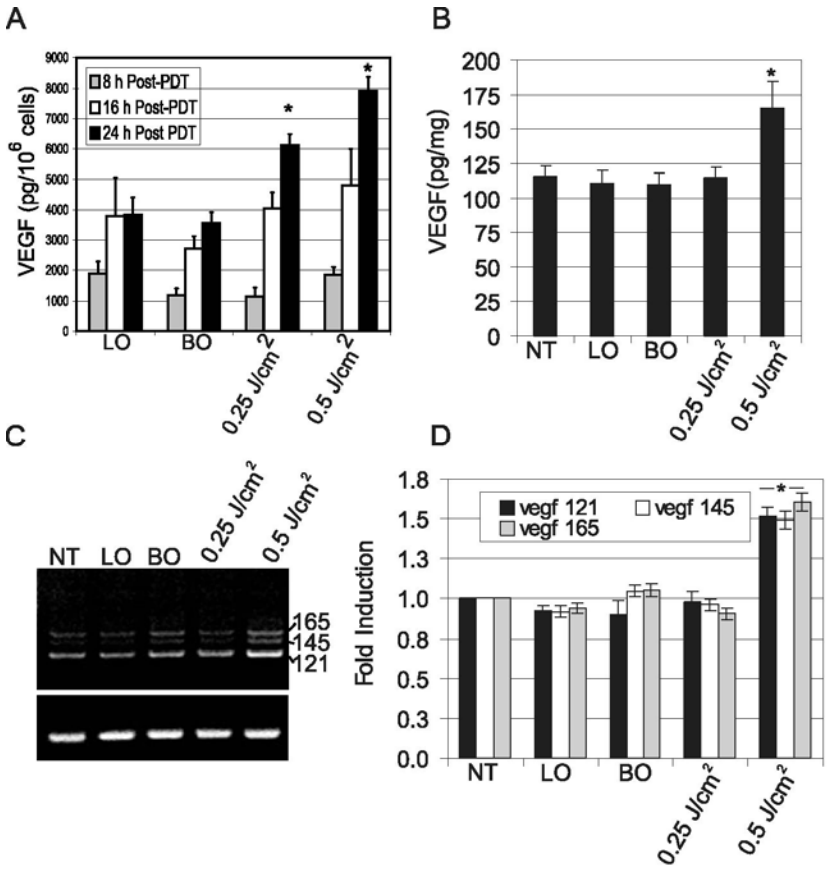

Figure 5: PSMA is expressed only in LNCaP cells. Western blot analysis shows expression of PSMA only in LNCaP cells both *in vitro* and *in vivo.* PDT treatment does not modify PSMA expression. PSMA is not detected in MLL cells.

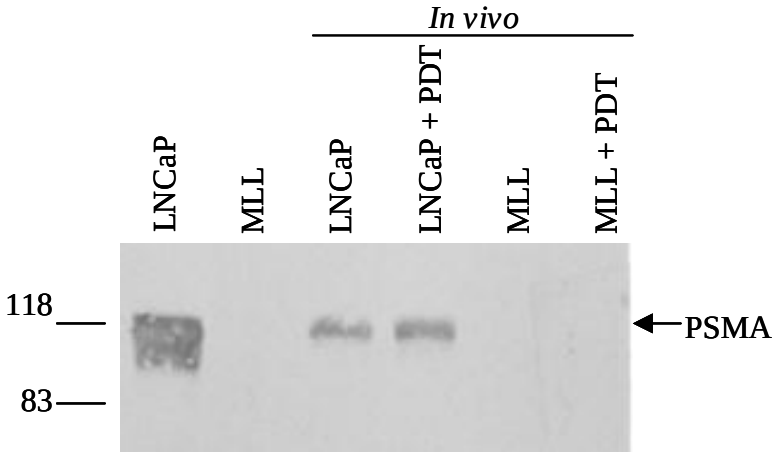

Figure 6: Specific labeling of LNCaP cells with PSMA-Cy5.5. LNCaP and MLL cells were incubated with 5 µg PSMA-Cy5.5 for 15 min at 37°C. After PBS washes cells were observed using a confocal microscope. LNCaP cells are specifically labeled while no labeling is observed in MLL cells.

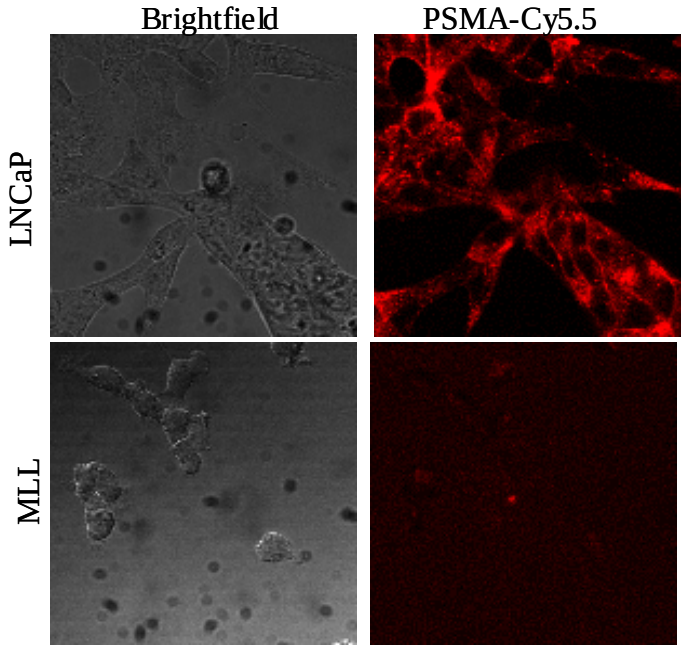

Figure 7: FACS Analysis of LNCaP cells. LNCaP cells were incubated with PSMA, PSMA-Cy5 or PSMA-Qdots. Specific fluorescence is observed with Cy5 and Qdots.

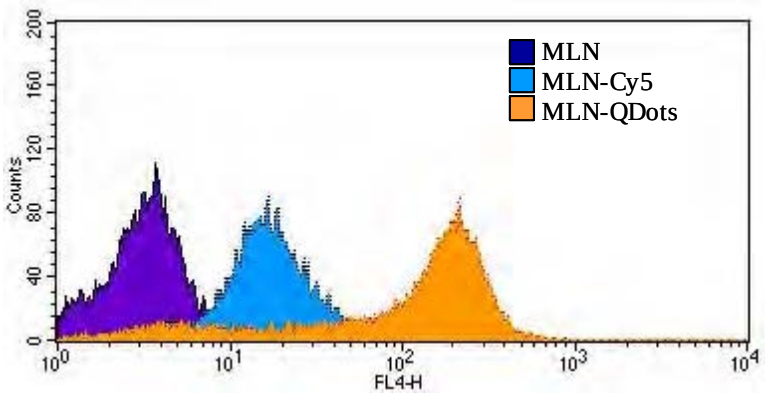

Figure 8: FACS analysis of GFP LNCaP and GFP MLL cells. Histogram of LNCaP-GFP and MLL-GFP before sorting. M1 represents cells with the highest fluorescence that were sorted. FL1-H is the channel used to detect green fluorescence.

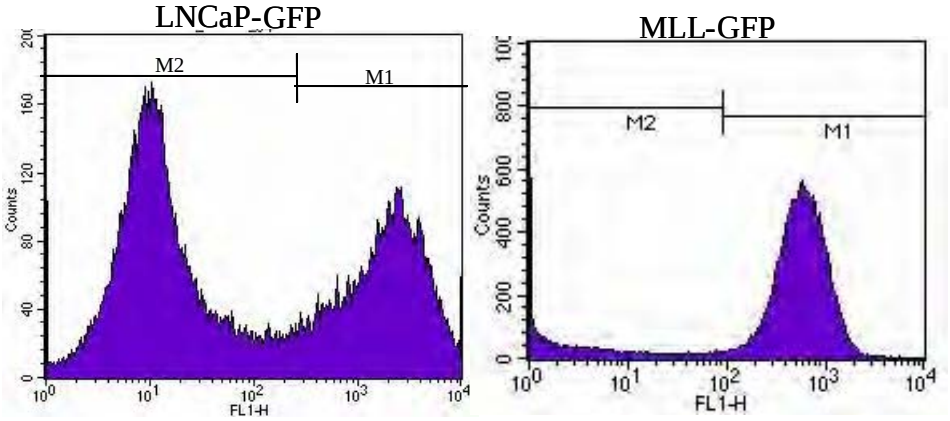

Figure 9. Subcurative PDT increases circulation time of prostate cancer cells. 24 h (-▲-) or 72 h (-■-) post-PDT or untreated (-◊-) MLL were labeled with the lipophilic dye DiD and injected in the tail vein of SCID mice and immediately placed on the IVFC. The normalized numbers of circulating cells per minute are shown for 3 h following injection of the fluorescently labeled cells. (n=3 with 5 measurements). * $P < 0.05$ when compared to untreated cells.

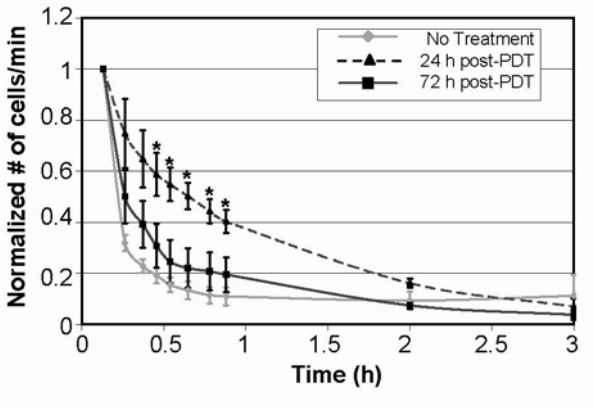

Figure 10: Immunohistochemical staining of β1 integrin in orthotopic prostate tumors. Microsections of tumors were stained with hematoxylin and eosin (H & E, top pictures) or with β1 integrin and hematoxylin (bottom figures). Arrow indicates area unaffected by treatment. NT: No treatment, PDT represents two different tumors.

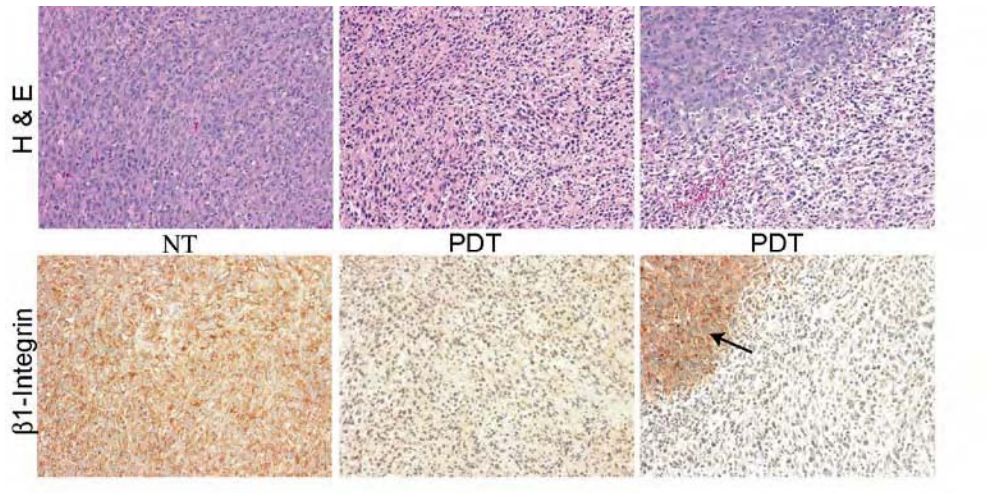

Figure 11: Analysis of β1 integrin and α5 integrin protein levels from orthotopic prostate tumors. 24 h following PDT, animals were sacrificed, tumors were collected and proteins and RNA were extracted. 100 μg or 25 μg of proteins was used for β1 integrin (A) and α5 integrin (B) western respectively. The level of actin was measured as a protein-loading control. PDT 1 and PDT 2 are proteins from tumors of 2 different animals. Graphs represent the average integrin β1 levels (left) or α5 levels (right) from 5 different tumors after calculating the integrin: actin ratio and performing densitometric analysis. Real-time RT-PCR analysis of β1 (C) and α5 (D) integrin mRNA levels. Results are expressed relative to NT and are mean ± SE of 5 independent experiments measured in triplicate. NT was arbitrarily set at 1. NT: No treatment, BO: BPD Only. ** $p < 0.001$, and * $p < 0.05$ when compared to NT.

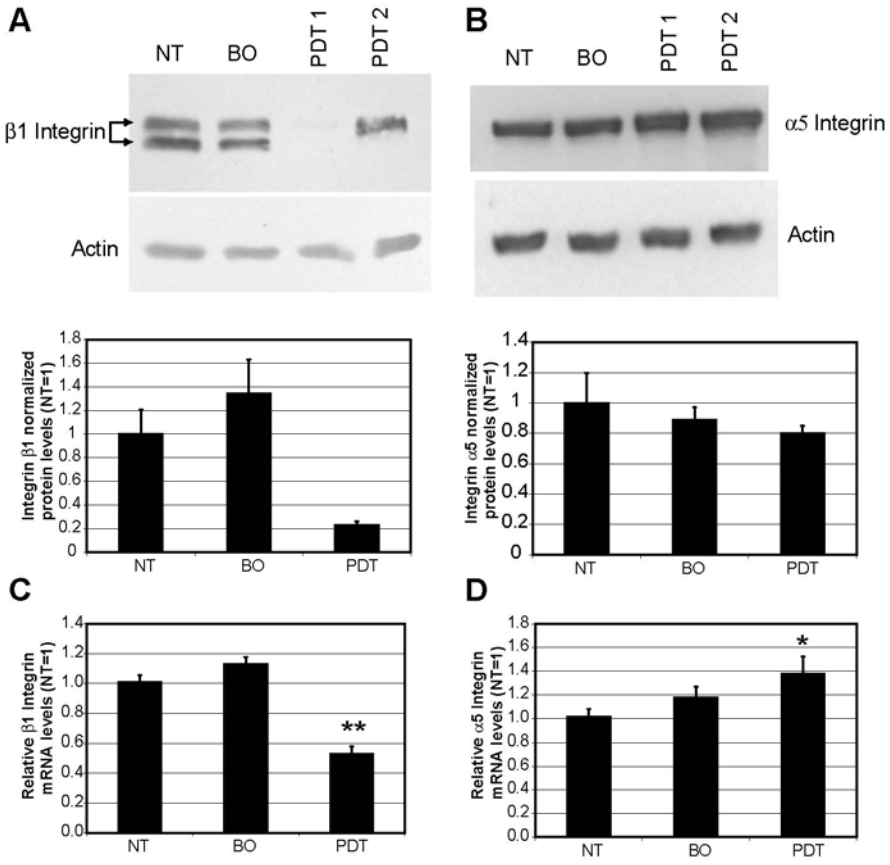

Figure 12: Immunohistochemical staining of VEGF protein in orthotopic prostate tumors. Microsections of tumors were stained with hematoxylin and eosin (*top pictures*) or with VEGF antibody and hematoxylin (*bottom figures*). A: No treatment. B: BPD only, C: PDT. Following subcurative PDT there is an increase in VEGF. Arrows indicate area of cell death and red blood cells infiltration indicative of vascular destruction (C). (20x magnification).

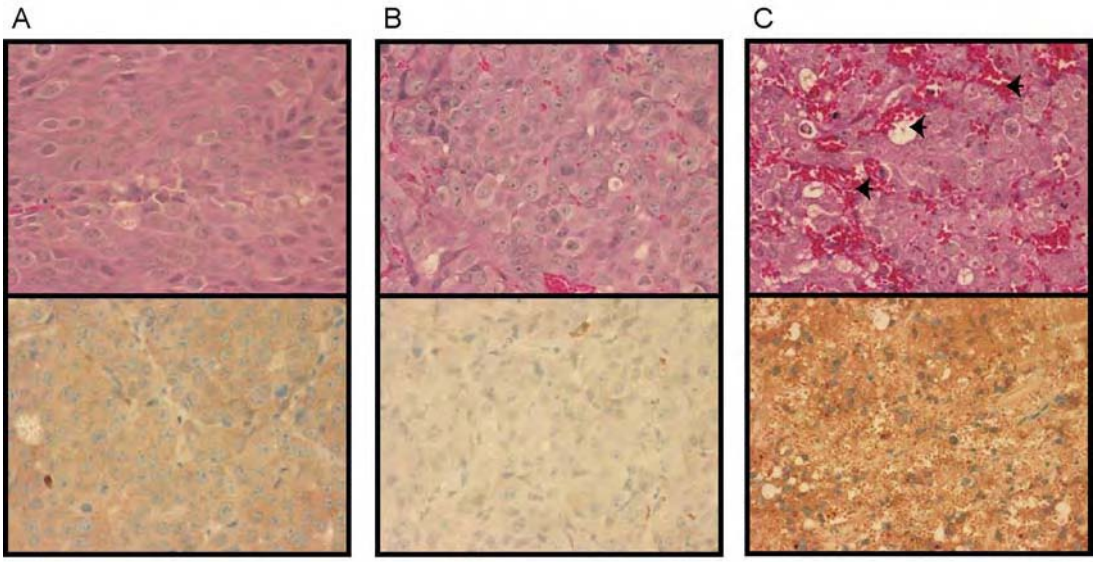

Figure 13: *In vivo* PDT increases VEGF. A) 24 h following treatment, orthotopic prostate tumors were collected, proteins were extracted and VEGF levels were measured by ELISA. Values are normalized relative to protein concentration and represent the mean ± SE of six animals for each group. A statistically significant increase (*, P<0.05) was measured following PDT. NT: no treatment, BO: BPD only.

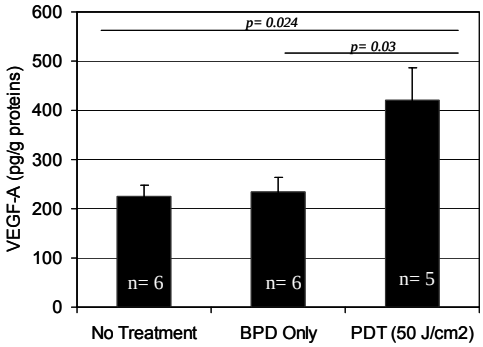

Figure 14: Treatment protocols. Orthotopic implantation of LNCaP cells in the prostate was done on day 1 and all animals were sacrificed on day 40. (A) Absolute control (n = 5). (B) PDT alone (n = 7). (C) TNP-470 alone (n = 5). (D) TNP-470 treatment preceding PDT (n = 8), (E) PDT followed by TNP-470 treatment (n = 5). TNP-470 was injected at 30 mg/kg body weight every 2 days for 1 week. PDT was done with 0.25 mg/kg liposomal BPD injected 1 h prior to light irradiation (100 J/cm^2). N = number of animals in each groups.

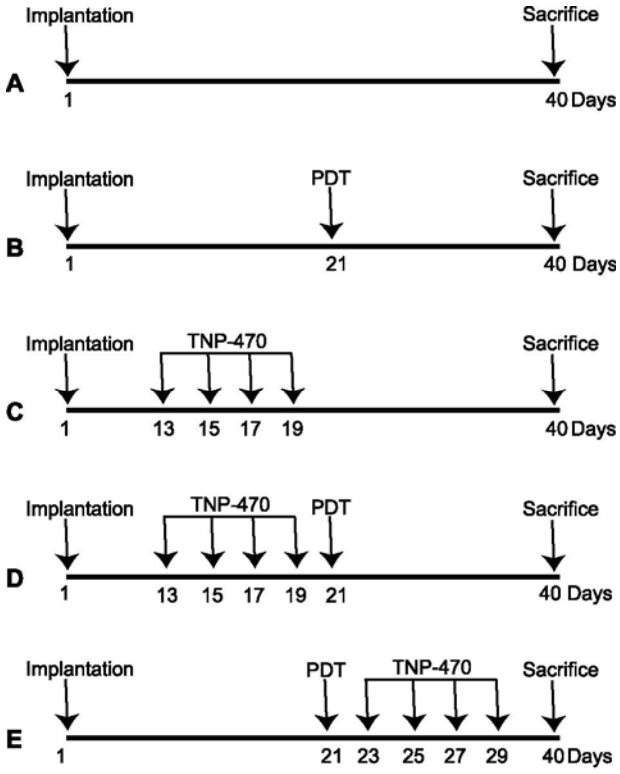

Figure 15: Combination treatment improves local tumor control and reduces metastases. (A) Animals from each group were euthanized 40 days following tumor cell implantation. The prostate, comprised of both normal and tumor tissue, was weighed. There is a significant decrease (*, $P < 0.05$) in prostate weight in the PDT + TNP-470 group only when compared to the control. (B) At the time of sacrifice lymph nodes were collected, fixed in 10 % formalin, and embedded in paraffin. Sections were cut throughout the lymph node and assessed for metastases. N = number of animals in each groups.

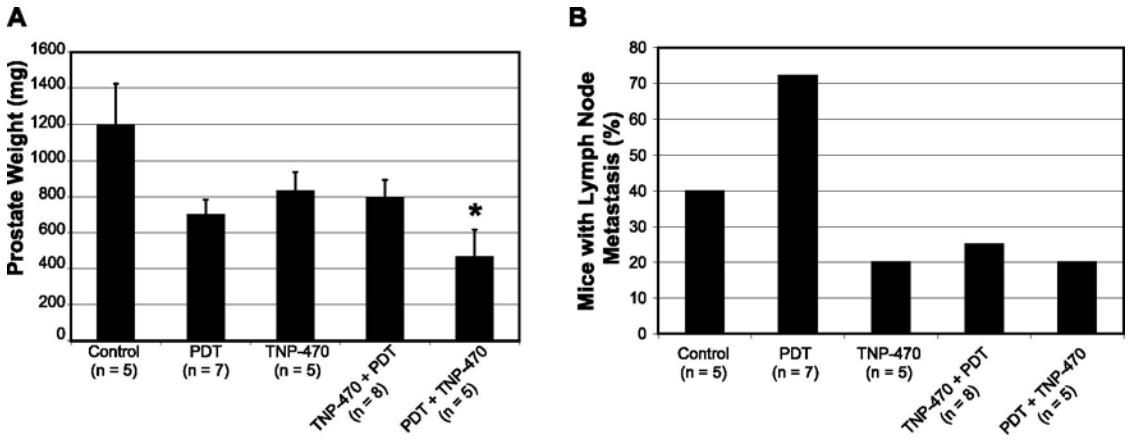

Mechanistic Investigation and Implications of Photodynamic Therapy Induction of Vascular Endothelial Growth Factor in Prostate Cancer

Nicolas Solban,[1] Selbo K. Pål,[2] Sinha K. Alok,[1] Chang K. Sung,[1] and Tayyaba Hasan[1]

[1]Wellman Center for Photomedicine, Massachusetts General Hospital, Harvard Medical School, Boston, Massachusetts and [2]Department of Radiation Biology, Institute for Cancer Research, The Norwegian Radium Hospital, Montebello, Oslo, Norway

Abstract

Photodynamic therapy (PDT) is now an approved therapeutic modality, and induction of vascular endothelial growth factor (VEGF) following subcurative PDT is of concern as VEGF may provide a survival stimulus to tumors. The processes that limit the efficacy of PDT warrant investigation so that mechanism-based interventions may be developed. This study investigates VEGF increase following subcurative PDT using the photosensitizer benzoporphyrin derivative (BPD) both in an *in vitro* and in an orthotopic model of prostate cancer using the human prostate cancer cell line LNCaP. The two subcurative doses used, 0.25 and 0.5 J/cm^2, mimicked subcurative PDT and elicited a 1.6- and 2.1-fold increase, respectively, in secreted VEGF 24 hours following PDT. Intracellular VEGF protein measurement and VEGF mRNA showed a 1.4- and 1.6-fold increase only at 0.5 J/cm^2. *In vivo* subcurative PDT showed an increase in VEGF by both immunohistochemistry and ELISA. *In vitro* analysis showed no activation of hypoxia-inducible factor-1α (HIF-1α) or cyclooxygenase-2 (COX-2) following subcurative PDT; furthermore, small interfering RNA inhibition of HIF-1α and COX-2 inhibitor treatment had no effect on PDT induction of VEGF. PDT in the presence of phosphatidylinositol 3-kinase/AKT inhibitor or mitogen-activated protein kinase (MAPK)/extracellular signal-regulated kinase inhibitor still induced VEGF. However, subcurative PDT increased phosphorylated p38 and stress-activated protein kinase/c-Jun NH_2-terminal kinase. The p38 MAPK inhibitor abolished PDT induction of VEGF. The results establish the importance of VEGF in subcurative BPD-PDT of prostate cancer and suggest possible molecular pathways for its induction. These findings should provide the basis for the development of molecular-based interventions for enhancing PDT and merit further studies. (Cancer Res 2006; 66(11): 5633-40)

Introduction

Photodynamic therapy (PDT) is an evolving technology that is approved as a first line treatment for age-related macular degeneration and for a variety of cancers (1). PDT consists of the systemic or local administration of a photosensitizer, its preferential accumulation in malignant tissues, and its subsequent activation by visible light. In the presence of oxygen, this activated photosensitizer can generate reactive oxygen species that are toxic to the tumor (2, 3). With the use of modern fiber-optic systems and various types of endoscopy, light can now be targeted accurately to almost any part of the body for the treatment of tumors. Several thousand patients have already been treated with PDT for a variety of advanced neoplasms and have shown an improvement in their quality of life and a lengthened survival (3, 4). For early and localized disease, PDT has also been shown to be a selective and curative therapy. Porfimer sodium (Photofrin) is approved for use in advanced and early stage lung cancers, superficial gastric cancer, esophageal adenocarcinoma, cervical cancer, bladder cancer, and Barrett's esophagus. Temoporfin, another photosensitizer, is approved in Europe for the palliative treatment of head and neck cancer. Although no other systemically administered photosensitizers are currently approved for the treatment of neoplasms, topically applied photosensitizers are approved for the treatment of actinic keratosis and basal cell carcinomas.

Today, PDT is being considered not only as palliative therapy but also as a treatment option for early lung cancer, actinic keratosis, and basal cell carcinoma. Currently, the use of PDT for localized disease and precancerous lesions is under investigation for bladder cancer, pituitary tumors, and glioblastoma (3, 4). The feasibility of using PDT for the treatment of localized recurrent prostate cancer has also been shown previously (5, 6). Furthermore, numerous ongoing clinical studies have been designed for the optimization of PDT conditions. As PDT becomes more of a mainstream treatment option for early cancers, it is important to understand factors that might counteract its tumoricidal effect. Our group is interested in studying the molecular responses of cancer cells that have been exposed to both photosensitizer and light but not in sufficient quantities to kill them. An understanding of these molecular responses will help in the design of new mechanism-based interventions and potentially improve long-term survival of PDT-treated patients.

An inherent consequence of PDT is local hypoxia. This condition can arise directly from oxygen consumption during treatment (7–9) or indirectly from the destruction of the tumor vasculature as a result of effective treatment (10, 11). Hypoxia is the major stimulus for angiogenesis through its stabilization of the transcription factor hypoxia-inducible factor-1α (HIF-1α; ref. 12), which is then able to bind to the HIF-1α response element (HRE; ref. 13) in the promoter of numerous genes, including in the promoter of the *vascular endothelial growth factor* (*VEGF*) gene, a potent angiogenic molecule, resulting in an increase in VEGF production and secretion (14). Following PDT, an increase in VEGF secretion (15, 16) as well as an angiogenic response has been documented (17, 18) *in vivo*. Ferrario et al. have shown an increase in HIF-1α following Photofrin-mediated PDT of a s.c. BA mouse mammary carcinoma (16) as well as an increase in cyclooxygenase-2 (COX-2) following PDT (19), leading to an increase in VEGF. However, the

Requests for reprints: Tayyaba Hasan, Wellman Center for Photomedicine, Massachusetts General Hospital, 40 Blossom Street, Boston, MA 02114. Phone: 617-726-6996; Fax: 617-726-8566; E-mail: thasan@partners.org.

doi:10.1158/0008-5472.CAN-06-0604

molecular mechanism of this PDT-induced VEGF increase may involve multiple pathways and may be system dependent (cell, tumor type, tumor model, or photosensitizer). Importantly, the host microenvironment can have profound effects on tumor physiology and expression of cellular molecules (20). A recent report by Chen et al. (21) of a rat prostate cancer model showed that s.c. tumors had reduced vascular density, VEGF secretion, and uptake of photosensitizer when compared with orthotopic tumors. In general, although sometimes difficult to generate, orthotopic models more adequately mimic physiologic conditions and are thought to be of more clinical relevance (22).

In the current study, we investigated the subcurative benzoporphyrin derivative (BPD)-PDT-based induction of VEGF *in vitro* and *in vivo* in an orthotopic model of prostate cancer using the human prostate cancer cell line LNCaP. Our results indicate that subcurative treatment induces VEGF synthesis and release both *in vitro* and *in vivo*. Somewhat surprisingly, our *in vitro* study shows that, in contrast to previously published data (16, 19, 23), this increase is independent of HIF-1α and COX-2 but was induced by the p38 mitogen-activated protein kinase (MAPK) signaling pathway. Due to the complexity of the disease process in cancer, single treatment modalities may not be highly effective; it is likely that rationally designed, mechanism-based combinations will offer greater chances of success. The results in this study establish the molecular pathway for subcurative BPD-PDT induction of VEGF in prostate cancer cells and should be useful in the development of molecular-based interventions for enhancing photodynamic treatment response. Furthermore, these results suggest that the molecular responses elicited by PDT are system specific and determined by many factors, such as the photosensitizer, cell type, tumor physiology, and photosensitizer localization at the time of treatment.

Materials and Methods

Cell culture and reagents. LNCaP cells, human prostate carcinoma cells, were obtained from the American Type Culture Collection (Rockville, MD). Monolayer cultures were incubated in RPMI 1640 (Mediatech, Herndon, VA) supplemented with 10% FCS (Invitrogen, Carlsbad, CA), 100 units/mL penicillin, 100 μg/mL streptomycin (Mediatech), and 10 mmol/L HEPES. BPD (140 nmol/L) was used in all *in vitro* assays, and liposomal BPD (0.25 mg/kg body weight) was used in all *in vivo* studies. BPD and liposomal BPD were donated by QLT, Inc. (Vancouver, British Columbia, Canada). LY 294002 [phosphatidylinositol 3-kinase (PI3K)/AKT inhibitor], SP 600125 [c-Jun NH_2-terminal kinase (JNK) inhibitor], SB 202190 (p38 MAPK inhibitor), and PD 98059 (p44/42 inhibitor) were purchased from Calbiochem (San Diego, CA). NS-398 (COX-2 inhibitor) was purchased from Sigma-Aldrich (St. Louis, MO).

Tumor implantation. Experiments were carried out on 6-week-old male severe combined immunodeficient mice weighing ~25 g (Cox Breeding Laboratories, Cambridge, MA). Animals were anesthetized with a 7:1 mixture of ketamine/xylazine. A 2-cm longitudinal incision from the pubic bone in a cranial direction exposed the prostate after the bladder was retracted cranially. LNCaP cells (3×10^6) in 50% Matrigel (BD Biosciences, San Diego, CA) were injected into the stroma of the prostate ventral lobe (0.1 mL total injection volume). The incision was closed with 2-0 suture. Three weeks following injection, a 0.1- to 0.2-cm^3 tumor develops.

Western blotting. LNCaP cells were resuspended in lysis buffer containing protease inhibitors (1% PBS, 1% NP40, 0.5% sodium deoxycholate, 0.1% SDS, 10 mg/mL phenylmethylsulfonyl fluoride, 100 mmol/L sodium orthovanadate, protease inhibitors). The LNCaP cells were incubated on ice for 30 minutes with vortexing every 5 minutes and then centrifuged at 14,000 rpm for 10 minutes at 4°C. The protein concentration was then determined using the standard Lowry method. Equal amounts of protein were separated by SDS-PAGE, blotted on polyvinylidene difluoride membrane, and probed with phosphorylated MAPK family antibody sampler kit (Cell Signaling Technology, Danvers, MA) or MAPK family antibody sampler kit (Cell Signaling Technology).

BPD localization. *In vivo* imaging: liposomal BPD localization in prostate tumors was imaged 1 hour after injection of 1 mg/kg BPD using a microscope coupled to a high-sensitivity CCD camera (Cascade:512F, Photometrics, Tucson, AZ). The microscope is composed of (*a*) 455-nm blue light-emitting diode (Luxeon LXHL-MRRC, Lumileds Lighting, San Jose, CA), (*b*) exciter filter (455/70, Chroma Technology, Rockingham, VT), (*c*) long-distance objective (Mitutoyo M Plan Apo 50×, Mitutoyo, Kawasaki, Japan), and (*d*) emitter filter (HQ700/75, Chroma Technology). Images were acquired with an exposure time of 200 ms/frame.

VEGF immunohistochemistry. Tumors were fixed in 10% formalin and embedded in paraffin. Tissue sections were deparaffinized, subjected to heat-induced epitope retrieval, immersed 30 minutes in 0.3% H_2O_2 to quench endogenous peroxidase activity, and blocked with normal mouse serum for 20 minutes (Vectastain avidin-biotin complex method kit, Vector Laboratories, Burlingame, CA). Sections were then incubated overnight at 4°C with VEGF antibody (Santa Cruz Biotechnology, Inc., Santa Cruz, CA), incubated with biotinylated secondary antibody for 30 minutes, incubated with avidin-peroxidase conjugate for 30 minutes, and stained with 3,3′-diaminobenzidine (DakoCytomation, Carpinteria, CA) for 3 minutes.

ELISA and reverse transcription-PCR. For intracellular VEGF measurements, proteins were extracted from orthotopic prostate tumors or from LNCaP cells. Briefly, frozen tumors were pulverized to powder in a tissue homogenizer and thawed in 1 mL/mg lysis buffer. LNCaP cells were resuspended directly in the lysis buffer. The protein concentration was determined using a standard Lowry method. For secreted VEGF measurements, cell medium was collected and centrifuged to remove cell debris. Viable cells were then counted using trypan blue. A human VEGF DuoSet ELISA Development System (R&D Systems, Minneapolis, MN) was used to quantify human VEGF levels. Results were normalized to protein concentrations or cell numbers.

Total RNA was extracted from LNCaP cells using the RNeasy Protect Mini kit (Qiagen, Inc., Valencia, CA) according to the manufacturer's instruction. Possible genomic DNA contamination was removed by RNase-free DNase I treatment (Qiagen). RNA concentration was estimated by reading the absorbance at 260 nm, and RNA integrity was shown by 1% agarose gel electrophoresis.

First-strand cDNAs were synthesized from 1 μg total RNA using Moloney murine leukemia virus reverse transcriptase (Invitrogen) and oligo(dT)15 Primer (Promega, Madison, WI) according to the manufacturer's instructions. Human VEGF-specific primers 5′-TCGGGCCTCCGAAACCATGA-3′ (forward) and 5′-CCTGGTGAGAGATCTGGTTC-3′ (reverse) were custom synthesized (Invitrogen) and used at 1 μmol/L each. The forward primer was located in the 5′-flanking region of exon 1 and the reverse primer in the 3′-open frame flanking region. PCR amplification with these primers could yield products of 772 bp ($VEGF_{206}$), 721 bp ($VEGF_{189}$), 649 bp ($VEGF_{165}$), 580 bp ($VEGF_{145}$), and 517 bp ($VEGF_{121}$). The following conditions were used: 94°C for 5 minutes followed by 30 cycles of amplification (94°C for 30 seconds, 58°C for 30 seconds, and 72°C for 30 seconds) and a final 72°C extension for 7 minutes. PCRs were electrophoresed through an ethidium bromide-stained 3% agarose gel. The bands were analyzed by densitometry. The housekeeping gene *glyceraldehyde-3-phosphate dehydrogenase* (*GAPDH*) was amplified as a control using the following primers: 5′-GTTCGACAGTCAGCCGCATG-3′ (forward) and 5′-GGAATTTGCCATGGGTGGA-3′ (reverse) at 0.2 μmol/L each. The PCR conditions used were the same as those described for the amplification of VEGF.

Photodynamic therapy. For *in vitro* PDT, 0.15×10^6 LNCaP cells were grown on a 35-mm culture dish for 24 hours and incubated with BPD (140 nmol/L) in 1 mL complete medium for 1 hour. Incubation medium was replaced with 2 mL fresh complete medium. Irradiation was done using a 690-nm diode laser (High Power Devices, Inc., North Brunswick, NJ). At 24 hours following irradiation, cell viability was measured using the 3-(4,5-dimethylthiazol-2-yl)-2,5-diphenyltetrazolium bromide assay (24). For *in vivo* PDT, liposomal BPD was injected in the tail vein of mice 1 hour

before irradiation. Before irradiation, a laparotomy was done and the prostate tumor was exposed. The tumor was irradiated at a fluence of 50 J/cm^2, with a fluence rate of 100 mW/cm^2. The incision was then closed. Twenty-four hours after treatment, the animals were euthanized and the tumors were collected.

Transfection and luciferase assay. For all transfections, 0.25×10^6 LNCaP cells in 35-mm dishes were transfected using Lipofectin (Invitrogen). At 24 hours after transfection, the cells were PDT treated. Twenty-four hours after treatment, cell medium was collected and analyzed by ELISA or cells were lysed and luciferase was measured using the Luciferase Assay System (Promega). Duplex HIF-1α RNA interference (RNAi) was designed using BLOCK-iT RNAi Designer (Invitrogen) as follows: 5′-CCAUGAGGAAAUGAGAGAAAUGCUU-3′ recognizes the open reading frame (ORF) of HIF-1α at position 704, a control duplex RNAi, based on the scrambled sequence of HIF-1α RNAi (5′-CCAAGGAGUAAGAGAUAAAGGUCUU-3′) was also designed. Both RNAi were ordered from Invitrogen, and 100 pmol were used for transfection.

Statistical evaluation. Data represented as mean ± SE of three independent experiments. A comparison of VEGF production by ELISA between PDT and light only or BPD only was calculated by unpaired Student's *t* test, and a mixed effects model for repeated measures analysis was used for *in vivo* measurements comparisons. $P < 0.05$ was considered statistically significant.

Results

VEGF Secretion and Transcription Are Increased by Sublethal PDT

In the LNCaP cells, BPD is localized in the mitochondria and also in the cytosol (data not shown). This extramitochondrial localization suggests that PDT could also affect cytoplasmic molecules. PDT of LNCaP cells with different light doses showed that LNCaP cells are highly susceptible to PDT killing. The very low light dose, 0.25 J/cm^2, kills ~10% of cells, whereas the 1.25 J/cm^2 dose kills ~90% of cells. To study the molecular response of cells that have been subjected to PDT but not enough to kill them, we chose the two subcurative doses, 0.25 and 0.5 J/cm^2. These doses kill ~10% and 40% of cells, respectively (data not shown). The time course analysis of VEGF release at 8, 16, and 24 hours following PDT with the two subcurative doses is presented in Fig. 1*A*; results were normalized to cell number. Treatment with 0.25 and 0.5 J/cm^2 led to a 1.6- and 2.1-fold increase ($P < 0.01$; Fig. 1*A*) in VEGF, respectively, when compared with light only or to BPD only 24 hours after treatment. Viability assay showed that cell death following BPD-PDT occurs before 8 hours and that the number of cells for each group does not significantly vary between 8 and 24 hours (data not shown). Furthermore, because there is no increase in VEGF after 8 or 16 hours (Fig. 1*A*), this suggests that the observed increase in VEGF following PDT is not due to the release of intracellular VEGF from dead cells.

To determine the mechanism of this increase, PDT-treated LNCaP cells were collected 24 hours following treatment, and intracellular VEGF levels were measured by ELISA. The results were normalized to protein concentration (Fig. 1*B*). A significant increase ($P < 0.05$) in intracellular VEGF at 0.5 J/cm^2 (1.4-fold) was observed (Fig. 1*B*). Surprisingly, despite an increase of VEGF in the cell-conditioned medium after the lower dose treatment (0.25 J/cm^2), there was no significant increase in the intracellular VEGF protein levels. To establish the mechanism of this increase, we used primers specific for exons 1 and 8 of the *VEGF* gene to determine VEGF mRNA levels following PDT. As described previously (25), these primers can amplify all possible isoforms of VEGF. Figure 1*C* shows a representative picture of a reverse

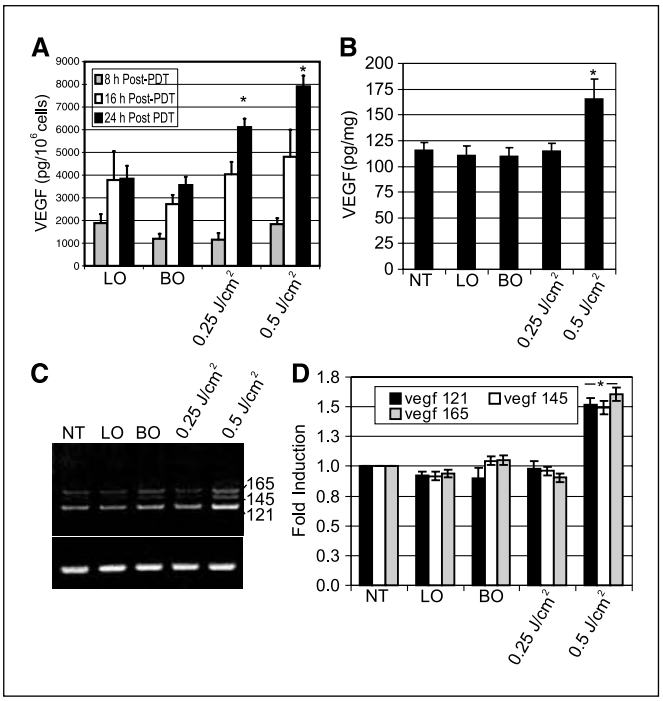

Figure 1. Increase of released and intracellular VEGF protein and mRNA following PDT. *A,* time course analysis of PDT induced VEGF release. At 8, 16, and 24 hours after PDT, secreted VEGF was measured by ELISA in the cell medium. Values are normalized relative to cell number. A statistically significant increase in secreted VEGF is measured 24 hours after PDT. *, $P < 0.01$, when compared with light only (*LO*) or to BPD only (*BO*). *B,* 24 hours after PDT, intracellular VEGF was measured by ELISA and a statistically significant increase was measured only with the 0.5 J/cm^2 light dose. *, $P < 0.05$, when compared with no treatment (*NT*), light only, or BPD only. Values are normalized relative to protein concentration. *C,* representative agarose gel analyzing RT-PCR products for VEGF (517, 580, and 649 bp corresponding, respectively, to the 121, 145, and 165 protein isoforms; *top gel*) or GAPDH (*bottom gel*). All VEGF isoforms are increased following 0.5 J/cm^2 treatment. *D,* relative levels of VEGF were determined by RT-PCR analysis. The results are expressed as fold induction of VEGF mRNA after calculating VEGF to GAPDH ratio. There is a statistically significant ~1.5-fold induction in all VEGF isoforms following 0.5 J/cm^2 treatment. *, $P < 0.01$, when compared with no treatment, light only, or BPD only. No treatment was arbitrarily set at 1. *Columns,* mean of three independent experiments; *bars,* SE.

transcription-PCR (RT-PCR) experiment following PDT. Only three isoforms of VEGF are expressed in LNCaP cells: $VEGF_{121}$, $VEGF_{145}$, and $VEGF_{165}$, with $VEGF_{121}$ being the most abundant and $VEGF_{145}$ being the least abundant. With the 0.5 J/cm^2 treatment, all three VEGF isoforms are increased (Fig. 1*C*). Figure 1*D* shows the average fold induction of each VEGF isoform following GAPDH normalization. All three isoforms detected are increased but only following the 0.5 J/cm^2 PDT. Concordant with intracellular protein levels, there is a significant ($P < 0.01$) increase in mRNA levels of $VEGF_{121}$, $VEGF_{145}$, and $VEGF_{165}$ (1.5-, 1.5-, and 1.6-fold increase, respectively, when compared with no treatment). However, because it is known that VEGF can be regulated at both transcriptional (26, 27) and post-transcriptional levels (27–29) from these experiments, we cannot exclude either mechanism.

In vivo Effects of PDT

To study the *in vivo* effect of subcurative PDT, we have used an orthotopic prostate cancer model that was shown to more reliably mimic pathologic conditions than ectopic models (21, 30, 31). Three weeks after LNCaP injection, a 0.1- to 0.2-cm^3 tumor will develop in 90% of cases. For *in vivo* studies, we have used the Food

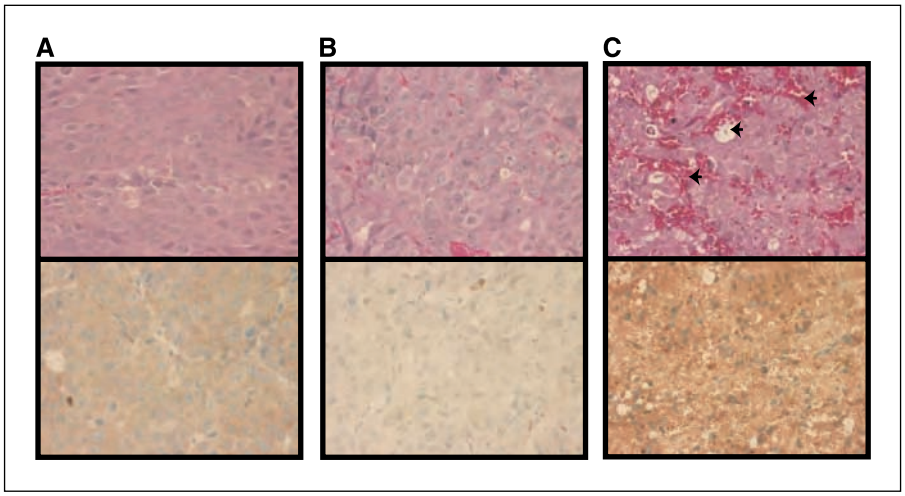

Figure 2. Immunohistochemical staining of VEGF protein in orthotopic prostate tumors. Microsections of tumors were stained with H&E (*top*) or VEGF antibody and hematoxylin (*bottom*). *A,* no treatment. *B,* BPD only, *C,* PDT. Following subcurative PDT, there is an increase in VEGF. *Arrows,* area of cell death and RBC infiltration indicative of vascular destruction (*C*). Magnification, ×20.

and Drug Administration–approved liposomal formulation of BPD (verteporfin) because tumor accumulation was shown to be increased *in vivo* when compared with its nonliposomal formulation (1). For subcurative treatment, light was delivered with a fluence rate of 100 mW/cm^2 and a total fluence of 50 J/cm^2. This treatment was shown to be subcurative but still causes significant tumor damage (data not shown). Therefore, it is ideal for the study of the response of tumors that have been exposed to both photosensitizer and light but not at sufficient levels to kill them. Immunohistochemical analysis of tumors collected 24 hours after treatment showed a more intense VEGF staining following PDT (Fig. 2, *bottom*; compare Fig. 2*C* to Fig. 2*A* and *B*). Figure 2 (*top*) shows the H&E staining of tumor sections. There were numerous necrotic areas observed after PDT (Fig. 2*C, top, arrows*) and a significant infiltration of RBC indicative of effective treatment. To have a more quantitative approximation of the VEGF increase, we collected proteins from tumors 24 hours after treatment. VEGF ELISA was done, and all results were normalized to protein concentration. This ELISA detects not only intracellular VEGF but also cell/extracellular-associated VEGF. There was a significant ($P < 0.05$) increase in VEGF levels following PDT (1.9-fold increase when compared with BPD only) in orthotopic prostate tumors (Fig. 3*A*), consistent with the immunohistochemical observations. *In vivo* imaging of BPD 1 hour after injection showed both a vascular and an intratumoral localization (Fig. 3*C, right*) of BPD. Therefore, with the experimental conditions used in this study, it is possible that hypoxia (vascular damage) and/or a direct effect of BPD may be responsible for the increase in VEGF following PDT.

Molecular Mechanisms Underlying PDT Induction of VEGF

Sublethal PDT increases transcription through a HIF-1α–independent mechanism. Hypoxia-induced stabilization of HIF-1α followed by its binding to the HRE in the *VEGF* promoter is a major regulator of *VEGF* gene expression (14). Because it is well documented that PDT consumes oxygen and can therefore generate hypoxic conditions *in vivo* (7–9, 11), we decided to evaluate the contribution of HIF-1α in the PDT induction of VEGF. LNCaP cells were transiently transfected with a luciferase-expressing plasmid under the control of the HRE (p5HRE-Luc). An increase in luciferase following PDT would indicate activation of HIF-1α; however, we did not measure any increase in luciferase 24 hours after treatment (data not shown). We have also measured luciferase activity at 4, 8, and 16 hours after PDT, but we did not detect any increase in luciferase at these various times either (data not shown). However, treatment with cobalt chloride, which has been shown to stabilize HIF-1α (12), induced a 2-fold increase in luciferase (data not shown). It is well established that HIF-1α activation can be rapid and transient (32), and it is possible that

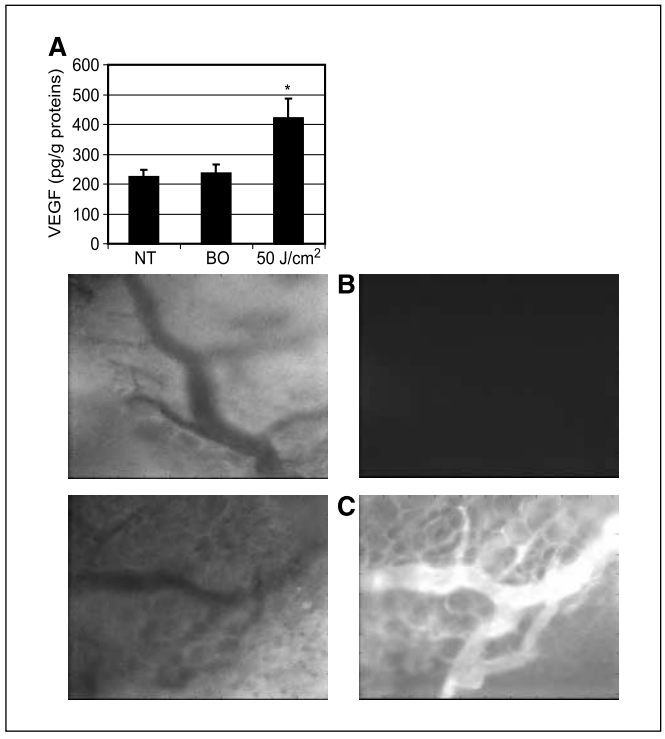

Figure 3. *In vivo* PDT increases VEGF. *A,* 24 hours following treatment, orthotopic prostate tumors were collected, proteins were extracted, and VEGF levels were measured by ELISA. Values are normalized relative to protein concentration. *Columns,* mean of six animals for each group; *bars,* SE. *, $P < 0.05$, a statistically significant increase was measured following PDT. *In vivo* localization of liposomal BPD 1 hour after injection in prostate tumors. *B* and *C, left,* autofluorescence imaging before and after photosensitizer injection, showing vasculature (*dark*). *B* and *C, right,* fluorescence imaging before and after photosensitizer injection, showing vascular and intratumoral fluorescence of liposomal BPD.

PDT activation of HIF-1α occurred transiently and below our threshold of detection. Consequently, we designed a RNAi to inhibit endogenous HIF-1α. HIF-1α RNAi recognizes the ORF of HIF-1α at position +704. We also designed a control RNAi based on the scrambled sequence of HIF-1α RNAi. Because the detection of the HIF-1α protein is difficult in LNCaP cells, we cotransfected LNCaP cells with p5HRE-Luc together with a HIF-1α expression plasmid and HIF-1α RNAi or control RNAi. We measured a 10-fold increase in luciferase activity with the HIF-1α expression vector and no effect of the control RNAi. On the other hand, this induction is abolished in the presence of HIF-1α RNAi, confirming the efficacy of our RNAi. No effect was observed with the HRE-independent plasmid pSV40-Luc. Next, we did PDT 24 hours after transfection of HIF-1α RNAi. Twenty-four hours after PDT, cell-conditioned medium was collected and assayed for VEGF. Figure 4*A* shows an increase in VEGF after PDT even in the presence of HIF-1α RNAi. Transfection efficiency in the presence of HIF-1α RNAi is ~90% (data not shown). Together, these results suggest a HIF-1α–independent mechanism of VEGF increase after PDT.

Subcurative PDT activation of VEGF through a MAPK pathway. It was recently shown that PDT could induce COX-2 and subsequently lead to an increase in VEGF (19, 23). However, Western blot analysis of COX-2 levels following subcurative PDT in the LNCaP cell lines did not show any induction (data not shown). We have also used the COX-2 inhibitor, NS-398, to test the contribution of COX-2 in VEGF induction after PDT. As shown in Fig. 4*B*, there is an increase in VEGF after PDT even in the presence of the COX-2 inhibitor, suggesting a different pathway for VEGF induction. It has also been shown that PDT can activate the PI3K/AKT pathway. Furthermore, this pathway can also lead to VEGF induction (33). Western blot analysis did not show any activation of this pathway at 30 minutes or 1, 2, or 24 hours (data not shown) after PDT in the LNCaP cell line. Furthermore, inhibition of the PI3K/AKT pathway with the specific inhibitor LY 294002 did not inhibit PDT induction of VEGF (Fig. 4*C*). Next, we evaluated the contribution of the MAPK pathways in PDT induction of VEGF. Western blot analysis using phosphorylation-specific MAPK antibodies showed an activation of the PI3K/JNK pathway and the p38 MAPK pathway at 30 minutes and 1 and 2 hours following treatment (Fig. 5*A*). No activation of the p44/42 MAPK pathway could be detected at any time point (data not shown). Finally, we used specific MAPK inhibitors to study VEGF induction after PDT. As expected, the p44/42 inhibitor (PD 98059) had no effect on VEGF synthesis (Fig. 4*D*). However, only the p38 MAPK inhibitor (SB 202190) inhibited VEGF synthesis after PDT (Fig. 5*C*), whereas the JNK inhibitor (SP 600125) had no effect on PDT induction of VEGF (Fig. 5*B*).

Discussion

PDT is an emerging modality for the treatment of various neoplastic and nonneoplastic pathologies. The feasibility of using PDT for the treatment of recurrent prostate cancer has previously been established (5, 6) and is now in early phase clinical trials (34). Most initial PDT-prostate cancer studies were interested in feasibility and efficacy (35). Due to the limited penetration depth of light in tissue and to the nonhomogenous distribution of the photosensitizer in the tumor, some areas receive suboptimal PDT (either not enough light or not enough photosensitizer or both). The relevance of the current study concerns suboptimal PDT, with our investigation of the biological response of tumor cells that have received sublethal PDT. Consistent with the findings of previous studies that showed that PDT induces VEGF in s.c. models (16), this study shows that sublethal and subcurative PDT induces VEGF secretion in LNCaP cell cultures as well as in an orthotopic model of prostate cancer.

In vivo experiments were done 1 hour after injection of liposomal BPD. At this specific time, the photosensitizer is localized in the

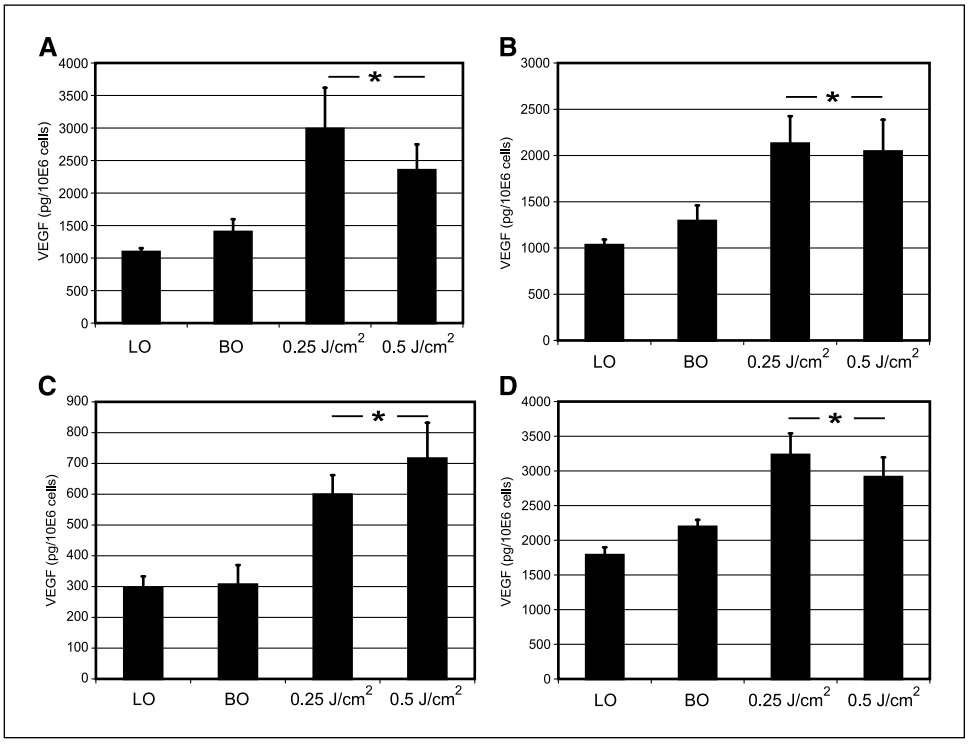

Figure 4. PDT increases VEGF in a HIF-1α-, COX-2-, AKT-, and p44/42-independent mechanism. *A,* to test the effect of HIF-1α on VEGF secretion following PDT, LNCaP cells were transfected with HIF-1α RNAi. Twenty-four hours after transfection, PDT was done. Twenty-four hours later, VEGF was measured using ELISA. There is an increase in VEGF secretion even in the presence of HIF-1α RNAi, suggesting a HIF-1α–independent mechanism of regulation. *B,* LNCaP cells were incubated with 10 μmol/L of the COX-2 inhibitor NS-398 or with 10 μmol/L of the AKT inhibitor LY 294002 (*C*) or with 10 μmol/L of the p44/p42 inhibitor PD 98059 (*D*) 24 hours before PDT. Twenty-four hours after PDT, VEGF was measured using an ELISA. Even in the presence of the inhibitors, there is an increase in VEGF secretion after PDT. *Columns,* mean of three independent experiments; *bars,* SE. *Asterisk,* statistically significant difference ($P < 0.01$) when compared with light only (*A-D*) and statistically significant difference ($P < 0.05$) when compared with BPD only for (*A, C*, and *D*).

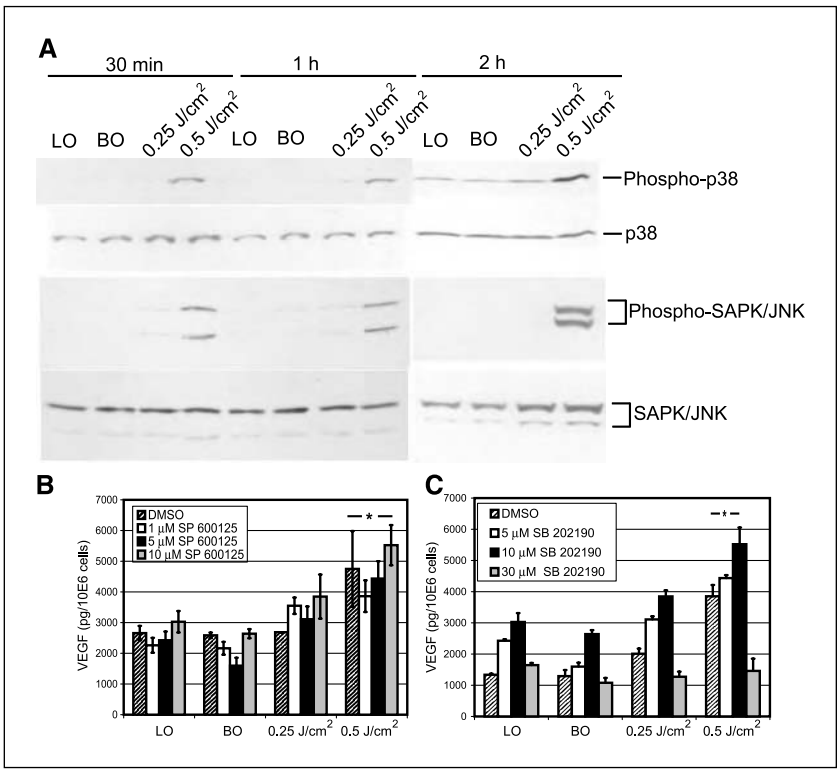

Figure 5. Subcurative PDT increases VEGF through a p38 MAPK pathway. Proteins were extracted 30 minutes and 1 and 2 hours following subcurative PDT of LNCaP cells. Equal amounts of protein lysates were assayed for the levels of phosphorylated p38 MAPK (*top*) or for phosphorylated SAPK/JNK. The levels of p38 MAPK and SAPK/JNK were also measured for total protein. *A,* there is an increase in phosphorylated p38 and in SAPK/JNK following PDT, indicating activation of the p38 MAPK and of the SAPK/JNK MAPK pathways. LNCaP cells were incubated with 1, 5, or 10 μmol/L of the SAPK/JNK inhibitor SP 600125 (*B*) or with 5, 10, or 30 μmol/L of the p38 MAPK inhibitor SB 202190 (*C*) for 24 hours before PDT. Twenty-four hours after PDT, VEGF was measured using an ELISA. PDT induction of VEGF was abolished only in the presence of the p38 MAPK inhibitor. *Columns,* mean of three independent experiments; *bars,* SE. *, $P < 0.05$, statistically significant difference when compared with light only or to BPD only.

vasculature but also starts to accumulate in the tumors (Fig. 3*C, right*). The localization of the photosensitizer at the time of irradiation is an important determinant of the mode of tumor destruction. In a recent study, Chen et al. (36) showed that BPD-PDT 15 minutes after injection of the photosensitizer induced endothelial cell damage, causing vascular leakage, thrombi formation, and, eventually, vascular shutdown. Therefore, a vascular photosensitizer at the time of treatment will induce vascular shutdown, efficiently starving the tumor, whereas an intratumoral photosensitizer will cause tumor cell apoptosis or necrosis (37). Consequently, subcurative PDT with a vascular photosensitizer could induce tumor hypoxia, leading to an increase in VEGF production. On the other hand, subcurative PDT with an intratumoral photosensitizer could induce signaling pathways, leading to VEGF increase. Therefore, PDT 1 hour following injection would lead to both direct tumor destruction and indirect destruction through vascular shutdown.

Studies by Ferrario et al. showed that tumoricidal action of PDT was enhanced by antiangiogenic treatment (16) and COX-2 inhibition (19, 23) initiated at the time of PDT. Inhibition of VEGF action was investigated in a separate study,[3] where the angiogenesis inhibitor, TNP-470, was used in combination with PDT to treat orthotopic prostate cancer models. We observed an increased in treatment efficacy in terms of both local control and distant metastasis. Taken together, these studies suggest that angiogenesis inhibition in combination with PDT improves therapeutic outcome. However, these studies also suggest that a mechanistic-based approach that directly inhibits VEGF secretion from cancer cells could have greater therapeutic potential.

On the mechanistic side, at a low PDT dose, VEGF increase is independent of protein synthesis, whereas, at the higher light dose, an increase in VEGF mRNA is observed (Fig. 1*B* and *D*). This suggests that the increase at the low light dose could be caused by the release of VEGF isoforms bound to the cell surface. Although there are no reports on the direct effect of PDT on proteoglycan, it is well documented that PDT can affect the cell membrane (38, 39). Subcellular localization of BPD showed not only a mitochondrial accumulation but also a cytosolic accumulation; it is therefore possible that activated BPD releases membrane-bound VEGF.

A single *VEGF* gene encodes multiple isoforms generated from alternative splicing (40). The *VEGF* gene contains 8 exons, and the various isoforms differ by the presence or absence of sequences encoded by exons 6 and 7. These isoforms differ in their ability to bind heparan sulfate proteoglycan found on cell surfaces as well as in the extracellular matrix (41). $VEGF_{121}$ does not bind to heparan sulfate proteoglycan and is freely secreted (42), whereas $VEGF_{145}$ and $VEGF_{165}$ are able to bind heparan sulfate proteoglycan and can be associated with the cell surface and extracellular matrix (41). We have shown that LNCaP cells express three of the VEGF isoforms: $VEGF_{121}$, $VEGF_{145}$, and $VEGF_{165}$ (Fig. 1*C*). It is therefore probable that some of the secreted VEGF remains bound to the surface of LNCaP cells.

To further probe the mechanism of VEGF induction and secretion, we investigated various cell signaling pathways that could contribute to an increase in VEGF. The first pathway investigated was the hypoxia-inducible pathway mediated by HIF-1α. It is well documented that *VEGF* can be regulated by this pathway under hypoxic conditions (14). Furthermore, because PDT is an O_2-consuming modality (7, 8) and an increase in HIF-1α has been previously reported by Ferrario et al. (16), this seemed like the most logical choice with which to start our investigation. Somewhat to our surprise, negative data were obtained with the

[3] Manuscript in preparation.

luciferase reporter plasmid and with HIF-1α RNAi. This excludes the possibility of the activation of HIF-1α by PDT, suggesting a HIF-1α–independent mechanism of VEGF secretion in LNCaP cells *in vitro*. A PDT induction of COX-2 that subsequently led to an increase in VEGF has previously been reported (19, 23). In contrast to these studies, we were not able to detect any COX-2 activation following PDT in the LNCaP cell line, and the use of a COX-2 inhibitor had no effect on the induction of VEGF following PDT. Our results suggest that, in the LNCaP cell line, the induction of VEGF is independent of COX-2. It is important to note that the study by Ferrario et al. used the photosensitizer Photofrin to treat a mouse mammary carcinoma, whereas, in our study, we used the photosensitizer BPD to treat a human prostate cancer. It is likely that different photosensitizer and different cell types induce VEGF via different pathways. These differences underscore the importance of the fact that PDT responses cannot be viewed as generic but are instead system specific. In fact, the specificity of the mechanistic pathways that lead to VEGF induction was further shown when the MAPK pathways were investigated.

VEGF is also under the control of MAPKs (26, 27), and because PDT has been shown to activate MAPKs (43, 44), we evaluated the activation of various MAPK family members following PDT in LNCaP cells. An increase in phosphorylated p38 and stress-activated protein kinase (SAPK)/JNK was measured following treatment but not in the p44/42 MAPK pathway. The use of specific MAPK inhibitors showed the involvement of the p38 MAPK pathway in the induction of VEGF following PDT. It has previously been shown that the p38 MAPK pathway as well as the SAPK/JNK pathway can increase VEGF mRNA stability (26, 27). Therefore, it is possible that the measured increase in VEGF mRNA is due to an increase in its stability.

Numerous studies have reported a biological response of cells following PDT, such as a decrease in cell adhesion (45, 46), an increase in cytokines production (47), and an increase in heat shock proteins (48). This study describes the effect of subcurative PDT on prostate cancer cells and reports an increase in VEGF both *in vitro* and *in vivo* in an orthotopic prostate cancer model. It was previously reported that COX-2 induces VEGF secretion (19, 23). However, in the prostate cancer cell lines, this increase is HIF-1α, COX-2, extracellular signal-regulated kinase, and AKT independent. On the other hand, subcurative PDT activates both the p38 MAPK and the SAPK/JNK pathway, but only inhibition of p38 MAPK abrogates PDT induction of VEGF secretion. The results shown establish the molecular pathway for subcurative PDT induction of VEGF in prostate cancer cells and should be useful in the development of molecular-based intervention for enhancing PDT. The best treatment outcomes from cancer treatments are increasingly recognized as resulting from combination treatments based on an understanding of molecular pathways that promote tumorigenesis (49). The details of the clinical relevance of the induction of VEGF by PDT are currently under investigation, but this induction could contribute to tumor survival and regrowth and therefore could be one of the factors impairing PDT from achieving its full tumoricidal potential. This deduction is supported by the improved tumor treatment response to PDT in combination with antiangiogenic agents (16, 50). In conclusion, rational combinations with appropriate mechanism-based interventions specific to the system being treated with PDT could significantly improve therapeutic outcomes.

Acknowledgments

Received 2/15/2006; revised 3/29/2006; accepted 4/5/2006.

Grant support: NIH grant P01 CA84203 (T. Hasan) and the Department of Defense grant PC040158 (N. Solban).

The costs of publication of this article were defrayed in part by the payment of page charges. This article must therefore be hereby marked *advertisement* in accordance with 18 U.S.C. Section 1734 solely to indicate this fact.

We thank QLT, Inc. for the gift of BPD and liposomal BPD, E. Davis for editorial help, and Dr. Y. Chang for statistical analysis.

References

1. Hasan T, Ortel B, Solban N, Pogue B. Photodynamic therapy of cancer. In: Kufe DW, Bast RC, Hait WN, Hong WK, Pollock R, Weichselbaum RR, Gansler T, Holland JF, Frei E III, editors. Cancer Medicine. 7th ed. Hamilton (Ontario, Canada): BC Decker, Inc.; 2006. p. 537–48.
2. Solban N, Ortel B, Pogue B, Hasan T. Targeted optical imaging and photodynamic therapy. Ernst Schering Res Found Workshop 2005;49:229–58.
3. Brown SB, Brown EA, Walker I. The present and future role of photodynamic therapy in cancer treatment. Lancet Oncol 2004;5:497–508.
4. Dougherty TJ. An update on photodynamic therapy applications. J Clin Laser Med Surg 2002;20:3–7.
5. Windahl T, Andersson SO, Lofgren L. Photodynamic therapy of localised prostatic cancer. Lancet 1990; 336:1139.
6. Nathan TR, Whitelaw DE, Chang SC, et al. Photodynamic therapy for prostate cancer recurrence after radiotherapy: a phase I study. J Urol 2002;168:1427–32.
7. Sitnik TM, Hampton JA, Henderson BW. Reduction of tumour oxygenation during and after photodynamic therapy *in vivo*: effects of fluence rate. Br J Cancer 1998; 77:1386–94.
8. Henderson BW, Busch TM, Vaughan LA, et al. Photofrin photodynamic therapy can significantly deplete or preserve oxygenation in human basal cell carcinomas during treatment, depending on fluence rate. Cancer Res 2000;60:525–9.
9. Chen Q, Huang Z, Chen H, Shapiro H, Beckers J, Hetzel FW. Improvement of tumor response by manipulation of tumor oxygenation during photodynamic therapy. Photochem Photobiol 2002;76:197–203.
10. Engbrecht BW, Menon C, Kachur AV, Hahn SM, Fraker DL. Photofrin-mediated photodynamic therapy induces vascular occlusion and apoptosis in a human sarcoma xenograft model. Cancer Res 1999;59:4334–42.
11. Fingar VH, Kik PK, Haydon PS, et al. Analysis of acute vascular damage after photodynamic therapy using benzoporphyrin derivative (BPD). Br J Cancer 1999;79: 1702–8.
12. Semenza GL. HIF-1 and mechanisms of hypoxia sensing. Curr Opin Cell Biol 2001;13:167–71.
13. Michel G, Minet E, Mottet D, Remacle J, Michiels C. Site-directed mutagenesis studies of the hypoxia-inducible factor-1α DNA-binding domain. Biochim Biophys Acta 2002;1578:73–83.
14. Forsythe JA, Jiang BH, Iyer NV, et al. Activation of vascular endothelial growth factor gene transcription by hypoxia-inducible factor 1. Mol Cell Biol 1996;16: 4604–13.
15. Deininger MH, Weinschenk T, Morgalla MH, Meyermann R, Schluesener HJ. Release of regulators of angiogenesis following hypocrellin-A and -B photodynamic therapy of human brain tumor cells. Biochem Biophys Res Commun 2002;298:520–30.
16. Ferrario A, von Tiehl KF, Rucker N, Schwarz MA, Gill PS, Gomer CJ. Antiangiogenic treatment enhances photodynamic therapy responsiveness in a mouse mammary carcinoma. Cancer Res 2000;60:4066–9.
17. Jiang F, Zhang ZG, Katakowski M, et al. Angiogenesis induced by photodynamic therapy in normal rat brains. Photochem Photobiol 2004;79:494–8.
18. Schmidt-Erfurth U, Schlotzer-Schrehard U, Cursiefen C, Michels S, Beckendorf A, Naumann GO. Influence of photodynamic therapy on expression of vascular endothelial growth factor (VEGF), VEGF receptor 3, and pigment epithelium-derived factor. Invest Ophthalmol Vis Sci 2003;44:4473–80.
19. Ferrario A, Von Tiehl K, Wong S, Luna M, Gomer CJ. Cyclooxygenase-2 inhibitor treatment enhances photodynamic therapy-mediated tumor response. Cancer Res 2002;62:3956–61.
20. Stephenson RA, Dinney CP, Gohji K, Ordonez NG, Killion JJ, Fidler IJ. Metastatic model for human prostate cancer using orthotopic implantation in nude mice. J Natl Cancer Inst 1992;84:951–7.
21. Chen B, Pogue BW, Zhou X, et al. Effect of tumor host microenvironment on photodynamic therapy in a rat prostate tumor model. Clin Cancer Res 2005;11:720–7.
22. Killion JJ, Radinsky R, Fidler IJ. Orthotopic models are necessary to predict therapy of transplantable tumors in mice. Cancer Metastasis Rev 1998-99;17:279–84.
23. Ferrario A, Fisher AM, Rucker N, Gomer CJ. Celecoxib and NS-398 enhance photodynamic therapy by increasing *in vitro* apoptosis and decreasing *in vivo* inflammatory and angiogenic factors. Cancer Res 2005;65:9473–8.
24. Merlin JL, Azzi S, Lignon D, Ramacci C, Zeghari N, Guillemin F. MTT assays allow quick and reliable measurement of the response of human tumour cells to photodynamic therapy. Eur J Cancer 1992;28A:1452–8.
25. Uthoff SM, Duchrow M, Schmidt MH, et al. VEGF isoforms and mutations in human colorectal cancer. Int J Cancer 2002;101:32–6.
26. Pages G, Pouyssegur J. Transcriptional regulation of

the vascular endothelial growth factor gene—a concert of activating factors. Cardiovasc Res 2005;65:564–73.
27. Mukhopadhyay D, Datta K. Multiple regulatory pathways of vascular permeability factor/vascular endothelial growth factor (VPF/VEGF) expression in tumors. Semin Cancer Biol 2004;14:123–30.
28. Pages G, Berra E, Milanini J, Levy AP, Pouyssegur J. Stress-activated protein kinases (JNK and p38/HOG) are essential for vascular endothelial growth factor mRNA stability. J Biol Chem 2000;275:26484–91.
29. Liu LX, Lu H, Luo Y, et al. Stabilization of vascular endothelial growth factor mRNA by hypoxia-inducible factor 1. Biochem Biophys Res Commun 2002;291:908–14.
30. Fukumura D, Yuan F, Monsky WL, Chen Y, Jain RK. Effect of host microenvironment on the microcirculation of human colon adenocarcinoma. Am J Pathol 1997; 151:679–88.
31. Monsky WL, Mouta Carreira C, Tsuzuki Y, Gohongi T, Fukumura D, Jain RK. Role of host microenvironment in angiogenesis and microvascular functions in human breast cancer xenografts: mammary fat pad versus cranial tumors. Clin Cancer Res 2002;8:1008–13.
32. Jewell UR, Kvietikova I, Scheid A, Bauer C, Wenger RH, Gassmann M. Induction of HIF-1α in response to hypoxia is instantaneous. FASEB J 2001;15:1312–4.
33. Zhong H, Chiles K, Feldser D, et al. Modulation of hypoxia-inducible factor 1α expression by the epidermal growth factor/phosphatidylinositol 3-kinase/PTEN/AKT/FRAP pathway in human prostate cancer cells: implications for tumor angiogenesis and therapeutics. Cancer Res 2000;60:1541–5.
34. Weersink RA, Bogaards A, Gertner M, et al. Techniques for delivery and monitoring of TOOKAD (WST09)-mediated photodynamic therapy of the prostate: clinical experience and practicalities. J Photochem Photobiol B 2005;79:211–22.
35. Zhu TC, Finlay JC, Hahn SM. Determination of the distribution of light, optical properties, drug concentration, and tissue oxygenation *in-vivo* in human prostate during motexafin lutetium-mediated photodynamic therapy. J Photochem Photobiol B 2005;79:231–41.
36. Chen B, Pogue BW, Luna JM, Hardman RL, Hoopes PJ, Hasan T. Tumor vascular permeabilization by vascular-targeting photosensitization: effects, mechanism, and therapeutic implications. Clin Cancer Res 2006;12:917–23.
37. Nowis D, Makowski M, Stoklosa T, Legat M, Issat T, Golab J. Direct tumor damage mechanisms of photodynamic therapy. Acta Biochim Pol 2005;52:339–52.
38. Specht KG, Rodgers MA. Plasma membrane depolarization and calcium influx during cell injury by photodynamic action. Biochim Biophys Acta 1991;1070: 60–8.
39. Kunz L, Stark G. Photofrin II sensitized modifications of ion transport across the plasma membrane of an epithelial cell line. I. Electrical measurements at the whole-cell level. J Membr Biol 1998;166:179–85.
40. Tischer E, Mitchell R, Hartman T, et al. The human gene for vascular endothelial growth factor. Multiple protein forms are encoded through alternative exon splicing. J Biol Chem 1991;266:11947–54.
41. Houck KA, Leung DW, Rowland AM, Winer J, Ferrara N. Dual regulation of vascular endothelial growth factor bioavailability by genetic and proteolytic mechanisms. J Biol Chem 1992;267:26031–7.
42. Cohen T, Gitay-Goren H, Sharon R, et al. VEGF121, a vascular endothelial growth factor (VEGF) isoform lacking heparin binding ability, requires cell-surface heparan sulfates for efficient binding to the VEGF receptors of human melanoma cells. J Biol Chem 1995; 270:11322–6.
43. Tao J, Sanghera JS, Pelech SL, Wong G, Levy JG. Stimulation of stress-activated protein kinase and p38 HOG1 kinase in murine keratinocytes following photodynamic therapy with benzoporphyrin derivative. J Biol Chem 1996;271:27107–15.
44. Tong Z, Singh G, Valerie K, Rainbow AJ. Activation of the stress-activated JNK and p38 MAP kinases in human cells by photofrin-mediated photodynamic therapy. J Photochem Photobiol B 2003;71:77–85.
45. Runnels JM, Chen N, Ortel B, Kato D, Hasan T. BPD-MA-mediated photosensitization *in vitro* and *in vivo*: cellular adhesion and β_1 integrin expression in ovarian cancer cells. Br J Cancer 1999;80:946–53.
46. Rousset N, Vonarx V, Eléouet S, et al. Effects of photodynamic therapy on adhesion molecules and metastasis. J Photochem Photobiol B Biol 1999;52:65–73.
47. Dougherty TJ, Marcus SL. Photodynamic therapy. Eur J Cancer 1992;28A:1734–42.
48. Luna MC, Ferrario A, Wong S, Fisher AM, Gomer CJ. Photodynamic therapy-mediated oxidative stress as a molecular switch for the temporal expression of genes ligated to the human heat shock promoter. Cancer Res 2000;60:1637–44.
49. Zhang Z, Li M, Rayburn ER, Hill DL, Zhang R, Wang H. Oncogenes as novel targets for cancer therapy (part I): growth factors and protein tyrosine kinases. Am J Pharmacogenomics 2005;5:173–90.
50. Zhou Q, Olivo M, Lye KY, Moore S, Sharma A, Chowbay B. Enhancing the therapeutic responsiveness of photodynamic therapy with the antiangiogenic agents SU5416 and SU6668 in murine nasopharyngeal carcinoma models. Cancer Chemother Pharmacol 2005; 56:569–77.

A mechanism-based combination therapy reduces local tumor growth and metastasis in an orthotopic model of prostate cancer.

Boleslav Kosharskyy[2#], Nicolas Solban[1#], Sung K Chang[1], Imran Rizvi[1], Yuchiao Chang[1], Tayyaba Hasan[1,*]

[#]B. Kosharskyy and N. Solban contributed equally to this work. [1]Wellman Center for Photomedicine, Massachusetts General Hospital, Harvard Medical School, Boston, Massachusetts. [2]Department of Anesthesiology, Mount Sinai Hospital, New York, NY.

Running Title: Combination therapy improves PDT treatment efficacy.

Key words: LNCaP, PDT, VEGF, Verteporfin, Photodynamic therapy

[*]Request for reprints: Tayyaba Hasan, Wellman Center for Photomedicine, Massachusetts General Hospital, 40 Blossom Street, Boston MA, 02114, Phone 617-726-6996; fax: 617-726-8566; E-mail: thasan@partners.org.

Acknowledgments

Grant support was provided by the National Institutes of Health: Grant P01 CA84203 and RO1 EB00664, and by the Department of Defense Grant PC040158 to N.S. during the preparation of this manuscript. We thank QLT Inc. for the gift of Verteporfin /BPD, Dr. J. Folkman for TNP-470, Dr. W. Beecken for help with the animal model, and E. Davis for editorial help.

Abbreviations

BPD: benzoporphyrin derivative.

PF: Photofrin®.

PDT: photodynamic therapy.

VEGF: vascular endothelial growth factor.

PS: photosensitizer.

HIF-1α: hypoxia inducible factor-1 α.

COX-2: cyclo-oxygenase-2

MAP kinase: mitogen activated protein kinase

PCa: prostate cancer

Abstract

Therapy-induced stimulation of angiogenic molecules can promote tumor angiogenesis leading to enhanced tumor growth and cancer metastasis. A number of standard and emerging therapies, such as radiation and photodynamic therapy (PDT), can induce angiogenic molecules, thus limiting their effectiveness. PDT is approved for the treatment of a number of cancers, however, its induction of VEGF creates conditions favorable to enhanced tumor growth and metastasis, therefore mitigating its cytotoxic and antivascular effects. This is the first report demonstrating that subcurative PDT in an orthotopic model of prostate cancer (LNCaP) not only increases VEGF secretion (2.1-fold), but also increases the fraction of animals with lymph node metastases. PDT followed by administration of an antiangiogenic agent, TNP-470, abolished this increase and reduced local tumor growth. On the other hand, administration of TNP-470 before PDT was less effective at local tumor control. In addition, animals in all groups except in the PDT + TNP-470 group, had a weight loss of > 3 g at the time of sacrifice; the weight of the animals in the PDT + TNP-470 group did not change. The significant reduction ($P < 0.05$) in tumor weight and volume observed between the PDT + TNP-470 group and the control group suggests that the combination of PDT and antiangiogenic treatment administered in the appropriate sequence was not only more effective at controlling local tumor growth and metastases, but also reduced disease-related toxicities. Such molecular response-based combinations merit further investigations as they enhance both monotherapies and lead to improved treatment outcomes.

Introduction

Photodynamic therapy (PDT) consists of the systemic or local administration of a photosensitizer (PS) and its subsequent activation by visible light. In the presence of oxygen, activated PS can generate reactive oxygen species that are toxic to the tumor (1, 2). With the use of modern fiber-optic systems and various types of endoscopy, light can now be targeted accurately to almost any part of the body, significantly increasing the number of PDT applications. PDT is approved as a first line treatment for Age Related Macular Degeneration and for a variety of cancers (3). Porfimer sodium (Photofrin®, PF) is approved for use in advanced and early-stage lung cancers, superficial gastric cancer, esophageal adenocarcinoma, cervical cancer, bladder cancer and Barrett's esophagus. Temoporfin, another PS, is approved in Europe for the palliative treatment of head and neck cancers. Topically applied photosensitizers are also approved for the treatment of actinic keratosis and basal cell carcinomas. PDT is also under investigation for the treatment of other neoplasias (2, 4), and the feasibility of using PDT for the treatment of localized recurrent prostate cancer has also been previously demonstrated and may be a viable treatment option (5-7).

As PDT becomes more of a mainstream treatment option for early cancers, it is important to understand the factors that might mitigate its tumoricidal effect. We have previously reported an increase in the number of lung metastases following subcurative BPD-PDT in a highly aggressive prostate cancer model (8). More recently, we and others have reported an increase in the synthesis and secretion of VEGF following subcurative PDT (9-11). The molecular responses of PDT-treated tumors have been investigated in order to design novel mechanism-based treatment regimens to improve PDT efficacy and long-term patient health. Along these lines, Ferrario et al. have shown an increase in HIF1-α following PF mediated PDT of a subcutaneous

BA mouse mammary carcinoma (12) and an increase in COX-2 following PDT (11) leading to an increase in VEGF. On the other hand, we recently showed that in the LNCaP prostate cancer cell line the VEGF increase following BPD-PDT occurred independently of HIF-1α and COX-2, but was induced by the p38 MAP kinase pathway (9). Taken together, these results suggest that tumor responses to PDT at the molecular level are not generic but probably depend on the tumor type, the site of implantation and the PS used for treatment. These observations prompted the current study, which to our knowledge, is the first report of the effect of subcurative PDT not only on VEGF induction, but also on lymph node metastasis in an orthotopic model of prostate cancer using the LNCaP cells, a human cell line.

In addition to the well documented increase in angiogenesis (13, 14) and in VEGF (9, 12) following subcurative PDT, many other molecules, such as IL-8, FGF 2, EGF, and PDGF can also promote angiogenesis (reviewed in (15)), and some of these cytokines are known to be upregulated following PDT *in vitro* (16, 17). In the current study we decided to use TNP-470, a molecule that inhibits the action of VEGF (angiogenesis), instead of a molecule specific to VEGF. TNP-470 is a synthetic analog of fumagillin, which strongly inhibits vascular endothelial cell proliferation and migration (18) by blocking methionyl aminopeptidase-2 (MetAP2). Furthermore, TNP-470 is under phase 1 clinical trial for the treatment of prostate cancer (19-21). We hypothesized that the combination of TNP-470 and PDT may improve local control and reduce metastasis.

Disease processes in cancer are complex, and single treatment modalities may not be totally effective. However, rationally designed, mechanism-based combination therapies, may have greater chance of success. The results presented in this study demonstrate that an understanding of factors that limit PDT efficacy could lead to novel combination therapies that

improve treatment outcome not only in terms of local tumor control but also by inhibiting metastasis and by reducing disease related toxicities.

Material and methods

Cell culture and reagents

LNCaP, human prostate carcinoma cells, were obtained from ATCC. Monolayer cultures were incubated in RPMI-1640 (Mediatech, Herndon, VA) supplemented with 10% FCS (Invitrogen, Carlsbad, CA), 100 units/ml penicillin, 100 μg/ml streptomycin (Mediatech, Herndon, VA) and 10 mM HEPES. 0.25 mg/kg body weight of liposomal BPD and 30 mg/kg body weight of TNP-470 was used in all *in vivo* studies. Liposomal BPD was donated by QLT Inc. (Vancouver, British Columbia, Canada), and the TNP-470 is a gift of Dr. Folkman.

Tumor Implantation

Experiments were carried out on 6-week-old male SCID mice weighing ~ 25 g (Cox Breeding Laboratories, Cambridge, MA). Animals were anesthetized with a 7:1 mixture of ketamine:xylazine. A 2-cm longitudinal incision from the pubic bone in a cranial direction exposed the prostate after the bladder was retracted cranially. Next 3×10^6 LNCaP cells in 50% Matrigel (BD Bioscience, San Diego, CA) were injected into the stroma of the prostate ventral lobe (total injection vol. 0.1 ml). The incision was closed with 2-0 sutures. Three weeks following injection, a 0.1~0.2 cm^3 tumor develops.

PDT

TNP-470 was injected on days 13, 15, 17, and 19 (for the TNP-470 group and for the TNP-470 + PDT group) or on days 23, 25, 27, and 29 (for the PDT + TNP-470 group) after the orthotopic implantation of the tumor cells while PDT was performed on day 21 after the implantation of cells. For PDT, Liposomal BPD was injected into the tail vein of mice 1 h prior to irradiation. Before irradiation, a laparotomy was performed and the prostate tumor was exposed. The tumor

was irradiated at a fluence of 100 J/cm^2 using a 690 nm diode laser (High Power Devices, Inc., North Brunswick, NJ). The incision was then closed. For ELISA, the animals were euthanized and the tumors were collected 24 hours after treatment (day 22). To evaluate the treatment response the animals were euthanized and the tumors were collected 40 days after implantation.

ELISA

For VEGF measurements, proteins were extracted from orthotopic prostate tumors 24 h following PDT treatment. Briefly, frozen tumors were pulverized to powder in a tissue homogenizer and thawed in 1 ml/mg lysis buffer containing protease inhibitors (1% PBS, 1% Nonidet P-40, 0.5% sodium deoxycholate, 0.1% SDS, 10 mg/ml PMSF, 100 mM sodium orthovanadate, and protease inhibitors). The protein concentration was determined using a standard Lowry method. A human VEGF DuoSet ELISA Development System (R&D Systems, Minneapolis, MN) was used to quantify human VEGF levels. Results were normalized to proteins.

Treatment response

Forty days after implantation, the animals were sacrificed by carbon dioxide asphyxiation. Pelvic lymph nodes, along with the entire prostate tissue, liver, and lungs, were removed. Prostate tissue was weighed. Lymph nodes and liver were fixed with 10% formalin for histological examination and identification of metastases. The lungs had Bouin's solution injected intratracheally, and were kept immersed for four days before the metastatic colonies were counted.

Analysis of micrometastases

Mice were sacrificed by CO_2 inhalation. The lymph nodes were removed and fixed in 10% formalin. The formalin-fixed lymph nodes were embedded in paraffin and serial sections (5 μm thick) were cut throughout each entire lymph node. Sections were stained with hematoxylin and eosin (H & E) using standard procedures. H & E stained lymph node sections were analyzed for tumor cells microscopically under 40× and 100× magnification. Tumor nodules were identified as densely packed large mitotic cells.

In vivo imaging

The fluorescently labeled molecule Alexa Fluor® 647-BSA (Invitrogen, Carlsbad, CA) was injected into the tail vein (0.125 mg) of anesthetized mice. Immediately following injection, a laparotomy exposed the prostate tumor, which was imaged using the Maestro *in vivo* imaging system (CRI, Inc, Woburn, MA). Twenty-one days after orthotopic implantation the tumors were imaged immediately before PDT, 24 h (day 22) and 96 h (day 24) following treatment; images were acquired every minute for the first 10 min and every 2 min for the final 10 min. To analyze the change in fluorescence with time, the tumor region in each image was divided into three non-overlapping areas. The three areas selected for each tumor were kept constant throughout the images acquired at different timepoints. Average fluorescence intensity per pixel was calculated from each of these three areas.

Statistical evaluation

Data was represented as the mean ± SE of three independent experiments. A comparison of VEGF production by ELISA between PDT and no treatment (NT), or BPD only (BO), was calculated by unpaired Student's *t* test, and a mixed effects model for repeated measures analysis was used for *in vivo* measurement comparisons. $P < 0.05$ was considered statistically significant.

Results

Subcurative PDT increases VEGF. LNCaP cells in 50% matrigel were injected in the prostate of male SCID mice. This orthotopic prostate cancer model has been well established in the laboratory, and three weeks following injection, a 0.1~0.2 cm^3 tumor develops in ~90% of animals injected. One hour prior to PDT, 0.25 mg/kg of liposomal BPD was injected intravenously. Laser irradiation was performed after a laparatomy exposed the tumor at a fluence of 100 J/cm^2. The following day the animals were sacrificed, the tumors were collected, and VEGF levels were quantified by ELISA (Figure 1). PDT induced a 2.1-fold increase in VEGF ($P < 0.05$) when compared to no treatment or to BPD only. In previous studies, under identical conditions, we did not observe any effect of light alone treatment (unpublished data and (22)). For this reasons we did not include a light only control.

Transient vascular shutdown following PDT. We have previously shown that 1 h following liposomal BPD injection, the photosensitizer is localized both in the vasculature and in the tumor (9). Furthermore, since PDT with vascular photosensitizers induces vascular shutdown, we decided to evaluate the functionality of the tumor vasculature following PDT. The fluorophore, Alexa Fluor® 647-BSA, was injected intravenously immediately before imaging the prostate tumor. Fluorescence in the untreated animal steadily increases over time (Figure 2, A, graph), suggesting that the fluorophore diffuses out of the tumor vasculature. Immediately after PDT (data not shown) as well as 24 h following treatment, no fluorescence is detected in the tumor, suggesting vascular shutdown (Figure 2, B, graph). However, 96 h following treatment, fluorescence can be detected in the tumor (Figure 2,C, graph), indicative of functional

vasculature. Interestingly, fluorescence levels do not increase as rapidly as in the untreated control animals (compare Figure 2,A to Figure 2,C), suggesting that the vasculature is less permeable.

Increased treatment efficacy when combining antiangiogenic therapy with PDT. It is well documented that VEGF is a potent angiogenic molecule (23, 24). Therefore, the measured increase in VEGF following PDT could reduce treatment efficacy by promoting tumor regrowth or potentially facilitating metastasis. For these reasons we decided to investigate the efficacy of combining the antiangiogenic molecule, TNP-470, with PDT. Figure 3 shows the various groups used in this study. Group D received TNP-470 every 2 days the week preceding PDT, while group E received TNP-470 every 2 days for the week following PDT. All animals were sacrificed 40 days following orthotopic implantation and the prostate, comprised of tumor tissue and normal tissue, was collected. The average weight loss and prostate volume for each group are shown in Table 1. The animals in all groups except group E had a weight loss of > 3 g, while the weight of animals in group E did not change. Weight loss was measured by subtracting weight at sacrifice to weight at time of implantation. A statistically significant difference ($P < 0.05$) in weight loss between the groups receiving PDT + TNP-470 and the control, PDT alone, and the TNP-470 + PDT group, could be measured. Prostate weight and prostate volume were also significantly reduced ($P < 0.05$) in the PDT + TNP-470 group when compared to the control group (Figure 4, A and Table 1). We did not measure any significant differences when TNP-470 was administered prior to PDT. It is important to note that, in the current study, we used subcurative PDT doses therefore the tumors at day 40 are > 400 mg compared to ~ 20 mg for normal prostate.

PDT increases the fraction of animals with lymph node metastases. At the time of sacrifice the lungs, pelvic lymph nodes, liver and spines were collected and metastatic spread was assessed. No metastases could be detected in the liver, spines and lungs in all groups. On the other hand, lymph node metastases were detected in some animals of every group. Figure 5 shows a representative picture of a lymph node with a metastatic nodule. Sections were cut throughout the entire lymph node and stained with H & E, and analyzed for metastases. Figure 4, B shows the percentage of animals with lymph node metastases for each group. Similar to our previous report (8), more animals from group B (72%), which received only PDT, had metastases when compared to all other groups. Interestingly, the fraction of animals with lymph node metastases was reduced in all TNP-470-treated groups.

Discussion

Photodynamic therapy is an emerging modality for the treatment of various neoplastic and non-neoplastic pathologies. Since PDT is a dynamic process the exact mechanism of tumor destruction and the accompanying molecular responses will depend on many factors including the light and photosensitizer dose, and the photosensitizer localization at the time of treatment. Depending on the exact parameters chosen, tumor destruction may be direct, from the induction of tumor cell apoptosis or necrosis (25), or indirect through vascular shutdown (26). The molecular responses of tumor cells to PDT may vary depending on the parameters used and may mitigate PDT efficacy.

The feasibility of using PDT for the treatment of recurrent prostate cancer has previously been established (6, 7), and is now in early phase clinical trials (5, 27). Due to the limited penetration depth of light in tissue and the non-homogenous distribution of the PS in the tumor, some areas receive suboptimal PDT (either not enough light or not enough PS, or both). Determining the molecular responses of these cells is therapeutically important as they may mitigate PDT efficacy. For example, an angiogenic response and an increase in metastases have been reported following subcurative PDT treatment (8, 13). Whether metastasis will be a problem in human studies is not clear at this point; however the current study and previous studies (12, 13) do suggest that subcurative PDT can create conditions favorable for tumor regrowth and metastasis. Using an orthotopic model of prostate cancer we present here the first report of subcurative PDT-induced increase of VEGF secretion accompanied by an increase in the incidence of lymph node metastases. Importantly the results show that if the angiogenic action of VEGF is blocked by the antiangiogenic peptide, TNP-470, tumor growth, lymph node metastasis and disease related toxicity are all reduced.

As with our earlier study (9), all these experiments were performed 1 h after injection of liposomal BPD. Under this specific condition, the PS was localized both in the vasculature and intratumorally. The localization of the PS at the time of irradiation is a critical determinant of the mode of tumor destruction. In a recent study, Chen et al. showed that BPD-PDT 15 min after PS injection induced endothelial cell damage, causing vascular leakage, thrombi formation, and eventually, vascular shutdown (28). Hence, a vascular PS at the time of treatment will induce vascular shutdown, efficiently starving the tumor, while an intratumoral PS will cause tumor cell apoptosis or necrosis (29). Therefore, the current PDT treatment protocol could lead to both direct tumor destruction and indirect destruction through vascular shutdown. Consistent with this paradigm, *in vivo* animal imaging showed rapid vascular shutdown following PDT. However 96 h following treatment, functional vasculatures are present in the tumor (Figure 2,C). The measured VEGF increase following PDT could play a part in the formation of these new vessels. The PDT dose used in the present study was twice that reported previously (9) since it might be argued that a higher PDT dose could reduce VEGF induction by more effective destruction of tumor tissue or by the direct photochemical destruction of the VEGF protein. However, we were still able to measure an increase of VEGF 24 h after PDT treatment. This suggests that, within the range of PDT doses used in the two studies, the VEGF increase is not strictly dependent on the light dose. At this point it is not clear which PDT conditions might prevent the secretion of VEGF but systematic studies on this aspect are ongoing. We are also evaluating the direct contribution of VEGF on tumor regrowth and metastasis, using Avastin®, a specific VEGF MAb shown to inhibit its function (30).

An emerging concept in antiangiogenic therapy involves the ‘normalization’ of tumor vessels. Antiangiogenic therapies have been proposed as initially improving the structure and

function of tumor vessels, resulting in an increase in tumor oxygenation. However, sustained treatment will eventually prune away tumor vessels, leading to hypoxia and potentially, tumor destruction (for review (31)). Studies using TNP-470 and minocycline to treat subcutaneously implanted gliosarcoma initially revealed a decrease in tumor hypoxia (32) and an increase in tumor oxygenation (33), compared to the untreated control. Similar observations were made with mouse mammary carcinomas (34). BPD-PDT is an oxygen dependant treatment modality. Once activated, BPD transfers its energy to oxygen to generate the highly toxic singlet oxygen. Furthermore, numerous studies have correlated an increase in treatment efficacy with increased tumor oxygenation (35, 36). We therefore tested the effect of administering TNP-470 for one week prior to PDT (Figure 3, group D). Compared with PDT alone, animals pretreated with TNP-470 tended to have a slightly higher prostate weight and prostate size (a measure of tumor burden). Although not significant, this difference could be due to the decrease in tumor vasculature, thereby limiting PS delivery. The best outcomes were obtained when TNP-470 was administered after PDT (Figure 3, group E) in order to inhibit the action of the PDT-induced angiogenic factors. This reduction of tumor burden is consistent with the hypothesis that TNP-470 interferes with the action of VEGF (or other angiogenic factors), thereby preventing tumor regrowth. It is also possible that PDT treated cells become more susceptible to TNP-470 treatment.

Mechanistic studies have established that TNP-470 blocks methionyl aminopeptidase-2 (MetAP2), an intracellular enzyme necessary for the process of protein myristolation, thus preventing membrane proteins from being translocated to the cell surface (37). This causes inhibition of endothelial cell proliferation by inhibiting their cell cycle progression (18, 38-40). However, since protein myristolation also occurs in other cell types, TNP-470 could have a

direct effect on the proliferation of tumor cells (41). However, in our experiments we did not observe a significant effect of TNP-470 treatment alone on prostate size and prostate weight when compared to the control group (Table 1 and Figure 4A). On the other hand, our results are consistent with the antiangiogenic action of TNP-470, although not necessarily demonstrative of antiangionesis.

LNCaP cells usually metastasize to the lymph node but can also metastasize to the lungs (42, 43). In a previous study an increase in lung metastases following subcurative PDT in an orthotopic rat prostate cancer model was reported (22). In this study we did not detect any lung metastases with the methods used in the study (Bouin's staining of perfused lungs). However, the presence of nodules not detectable by Bouin's solution is not ruled out. On the other hand, more animals in the PDT treated group had an increase in lymph node metastases, suggesting that subcurative PDT generates conditions favorable to metastatic spread. Furthermore the fraction of animals with lymph node metastases was reduced in all TNP-470-treated groups. This is consistent with the notion that the presence of the antiangiogenic molecule, TNP-470, could prevent the growth of colonized cells by inhibiting angiogenic support for the growing colonies, or directly by preventing the release of cells from the tumor, or both. Interestingly, when PDT treatment was curative we did not observe any increase in metastases (22), suggesting that only surviving cells can elicit conditions favorable to spreading. It is possible that the subcurative outcome is due to the non-homogenous distribution of the PS and/or of light in the tumor, suggesting that dosimetry measurements could improve treatment (44). The current study emphasizes the need for careful dosimetry in order to avoid partial responses that may have adverse long-term effects despite good local control.

In summary, this is the first report of inhibition of subcurative PDT-induced tumor growth and metastasis in an orthotopic model of cancer and suggests that the use of an angiogenic inhibitor such as TNP-470 (which could also have a direct tumor cell growth inhibitory effect) in combination with PDT could improve therapeutic outcomes in cancer patients and possibly reduce treatment related toxicities from a given monotherapy. This study also suggests that a mechanism-based approach that directly inhibits VEGF secretion could enhance the therapeutic potential (45) of both PDT and antiangiogenic treatments and merits further investigations.

References

1. Solban N, Ortel B, Pogue B, Hasan T. Targeted optical imaging and photodynamic therapy. Ernst Schering Res Found Workshop 2005;49:229-58.

2. Brown SB, Brown EA, Walker I. The present and future role of photodynamic therapy in cancer treatment. Lancet Oncol 2004;5:497-508.

3. Hasan T, Ortel B, Solban N, Pogue B. Photodynamic therapy of cancer. In: Kufe, Bast, Hait, Hong, Pollock, Weichselbaum, et al, editors. Cancer Medicine, 7th edition. Hamilton, Ontario: B.C. Decker, Inc; 2006. p. 537-548.

4. Dougherty TJ. An update on photodynamic therapy applications. J Clin Laser Med Surg 2002;20:3-7.

5. Verigos K, Stripp DC, Mick R, et al. Updated results of a phase I trial of motexafin lutetium-mediated interstitial photodynamic therapy in patients with locally recurrent prostate cancer. J Environ Pathol Toxicol Oncol 2006;25:373-88.

6. Windahl T, Andersson SO, Lofgren L. Photodynamic therapy of localised prostatic cancer. Lancet 1990;336:1139.

7. Nathan TR, Whitelaw DE, Chang SC, et al. Photodynamic therapy for prostate cancer recurrence after radiotherapy: A phase I study. J Urol 2002;168:1427-32.

8. Momma T, Hamblin MR, Wu HC, Hasan T. Photodynamic therapy of orthotopic prostate cancer with benzoporphyrin derivative: Local control and distant metastasis. Cancer Res 1998;58:5425-31.

9. Solban N, Selbo PK, Sinha AK, Chang SK, Hasan T. Mechanistic investigation and implications of PDT-induction of VEGF in prostate cancer. Cancer Res 2006;66:1-8.

10. Ferrario A, von Tiehl KF, Rucker N, Schwarz MA, Gill PS, Gomer CJ. Antiangiogenic treatment enhances photodynamic therapy responsiveness in a mouse mammary carcinoma. Cancer Res 2000;60:4066-9.

11. Ferrario A, Von Tiehl K, Wong S, Luna M, Gomer CJ. Cyclooxygenase-2 inhibitor treatment enhances photodynamic therapy-mediated tumor response. Cancer Res 2002;62:3956-61.

12. Ferrario A, von Tiehl KF, Rucker N, Schwarz MA, Gill PS, Gomer CJ. Antiangiogenic treatment enhances photodynamic therapy responsiveness in a mouse mammary carcinoma. Cancer Res 2000;60:4066-9.

13. Jiang F, Zhang ZG, Katakowski M, et al. Angiogenesis induced by photodynamic therapy in normal rat brains. Photochem Photobiol 2004;79:494-8.

14. Schmidt-Erfurth U, Schlotzer-Schrehard U, Cursiefen C, Michels S, Beckendorf A, Naumann GO. Influence of photodynamic therapy on expression of vascular endothelial growth factor (VEGF), VEGF receptor 3, and pigment epithelium-derived factor. Invest Ophthalmol Vis Sci 2003;44:4473-80.

15. Uehara H. Angiogenesis of prostate cancer and antiangiogenic therapy. J Med Invest 2003;50:146-53.

16. Adili F, Scholz T, Hille M, et al. Photodynamic therapy mediated induction of accelerated re-endothelialisation following injury to the arterial wall: Implications for the prevention of postinterventional restenosis. Eur J Vasc Endovasc Surg 2002;24:166-75.

17. Du H, Bay BH, Mahendran R, Olivo M. Endogenous expression of interleukin-8 and interleukin-10 in nasopharyngeal carcinoma cells and the effect of photodynamic therapy. Int J Mol Med 2002;10:73-6.

18. Ingber D, Fujita T, Kishimoto S, et al. Synthetic analogues of fumagillin that inhibit angiogenesis and suppress tumour growth. Nature 1990;348:555-7.

19. Logothetis CJ, Wu KK, Finn LD, et al. Phase I trial of the angiogenesis inhibitor TNP-470 for progressive androgen-independent prostate cancer. Clin Cancer Res 2001;7:1198-203.

20. Retter AS, Figg WD, Dahut WL. The combination of antiangiogenic and cytotoxic agents in the treatment of prostate cancer. Clin Prostate Cancer 2003;2:153-9.

21. Figg WD, Kruger EA, Price DK, Kim S, Dahut WD. Inhibition of angiogenesis: Treatment options for patients with metastatic prostate cancer. Invest New Drugs 2002;20:183-94.

22. Momma T, Hamblin MR, Wu HC, Hasan T. Photodynamic therapy of orthotopic prostate cancer with benzoporphyrin derivative: Local control and distant metastasis. Cancer Res 1998;58:5425-31.

23. Hrouda D, Nicol DL, Gardiner RA. The role of angiogenesis in prostate development and the pathogenesis of prostate cancer. Urol Res 2003;30:347-55.

24. Nicholson B, Theodorescu D. Angiogenesis and prostate cancer tumor growth. J Cell Biochem 2004;91:125-50.

25. Ahmad N, Mukhtar H. Mechanism of photodynamic therapy-induced cell death. Methods Enzymol 2000;319:342-58.

26. Wang HW, Putt ME, Emanuele MJ, et al. Treatment-induced changes in tumor oxygenation predict photodynamic therapy outcome. Cancer Res 2004;64:7553-61.

27. Weersink RA, Bogaards A, Gertner M, et al. Techniques for delivery and monitoring of TOOKAD (WST09)-mediated photodynamic therapy of the prostate: Clinical experience and practicalities. J Photochem Photobiol B 2005;79:211-22.

28. Chen B, Pogue BW, Luna JM, Hardman RL, Hoopes PJ, Hasan T. Tumor vascular permeabilization by vascular-targeting photosensitization: Effects, mechanism, and therapeutic implications. Clin Cancer Res 2006;12:917-23.

29. Nowis D, Makowski M, Stoklosa T, Legat M, Issat T, Golab J. Direct tumor damage mechanisms of photodynamic therapy. Acta Biochim Pol 2005;52:339-52.

30. Ferrara N. Vascular endothelial growth factor: Basic science and clinical progress. Endocr Rev 2004;25:581-611.

31. Jain RK. Normalization of tumor vasculature: An emerging concept in antiangiogenic therapy. Science 2005;307:58-62.

32. Teicher BA, Holden SA, Ara G, et al. Influence of an anti-angiogenic treatment on 9L gliosarcoma: Oxygenation and response to cytotoxic therapy. Int J Cancer 1995;61:732-7.

33. Teicher BA, Dupuis NP, Emi Y, Ikebe M, Kakeji Y, Menon K. Increased efficacy of chemo- and radio-therapy by a hemoglobin solution in the 9L gliosarcoma. In Vivo 1995;9:11-8.

34. Teicher BA, Holden SA, Dupuis NP, et al. Potentiation of cytotoxic therapies by TNP-470 and minocycline in mice bearing EMT-6 mammary carcinoma. Breast Cancer Res Treat 1995;36:227-36.

35. Henderson BW, Gollnick SO, Snyder JW, et al. Choice of oxygen-conserving treatment regimen determines the inflammatory response and outcome of photodynamic therapy of tumors. Cancer Res 2004;64:2120-6.

36. Togashi H, Uehara M, Ikeda H, Inokuchi T. Fractionated photodynamic therapy for a human oral squamous cell carcinoma xenograft. Oral Oncol 2006;42:526-32.

37. Sin N, Meng L, Wang MQ, Wen JJ, Bornmann WG, Crews CM. The anti-angiogenic agent fumagillin covalently binds and inhibits the methionine aminopeptidase, MetAP-2. Proc Natl Acad Sci U S A 1997;94:6099-103.

38. Yamamoto T, Sudo K, Fujita T. Significant inhibition of endothelial cell growth in tumor vasculature by an angiogenesis inhibitor, TNP-470 (AGM-1470). Anticancer Res 1994;14:1-3.

39. Zhang Y, Griffith EC, Sage J, Jacks T, Liu JO. Cell cycle inhibition by the anti-angiogenic agent TNP-470 is mediated by p53 and p21WAF1/CIP1. Proc Natl Acad Sci U S A 2000;97:6427-32.

40. Yeh JR, Mohan R, Crews CM. The antiangiogenic agent TNP-470 requires p53 and p21CIP/WAF for endothelial cell growth arrest. Proc Natl Acad Sci U S A 2000;97:12782-7.

41. Sedlakova O, Sedlak J, Hunakova L, et al. Angiogenesis inhibitor TNP-470: Cytotoxic effects on human neoplastic cell lines. Neoplasma 1999;46:283-9.

42. Wang X, An Z, Geller J, Hoffman RM. High-malignancy orthotopic nude mouse model of human prostate cancer LNCaP. Prostate 1999;39:182-6.

43. Sato N, Gleave ME, Bruchovsky N, Rennie PS, Beraldi E, Sullivan LD. A metastatic and androgen-sensitive human prostate cancer model using intraprostatic inoculation of LNCaP cells in SCID mice. Cancer Res 1997;57:1584-9.

44. Zhou X, Pogue BW, Chen B, et al. Pretreatment photosensitizer dosimetry reduces variation in tumor response. Int J Radiat Oncol Biol Phys 2006;64:1211-20.

45. Ferrario A, Gomer CJ. Avastin enhances photodynamic therapy treatment of kaposi's sarcoma in a mouse tumor model. J Environ Pathol Toxicol Oncol 2006;25:251-60.

Table

Table 1

Treatment response. Weight loss for animals (g) is calculated by subtracting weight at sacrifice to weight before injection. After sacrifice prostate weight (normal tissue + tumor tissue) was determined (mg) and the prostate volume (mm^3) was measured. N = number of animals in each group. For weight loss there is a statistically significant difference (*, $P < 0.05$) between PDT + TNP-470 and Control, PDT, and TNP-470 + PDT groups only. For prostate volume there is a statistically significant difference (*, $P < 0.05$) only between PDT + TNP-470 and Control.

Groups	Weight loss (mean ± SE)	Prostate volume (mean ± SE)
A) Control (n=5)	6.1 ± 0.5	761 ± 110
B) PDT (n=7)	5.4 ± 0.5	407± 134
C) TNP-470 (n=5)	3.1 ± 0.9	484 ± 94
D) TNP-470 + PDT (n=8)	4 ± 0.4	696 ± 170
E) PDT + TNP-470 (n=5)	-0.3 ± 0.9 *	277 ± 116 *

Figures

Figure 1

In vivo PDT increases VEGF. At 24 h following treatment, orthotopic prostate tumors were collected, proteins were extracted, and VEGF levels were measured by ELISA. Values are normalized relative to protein concentration and represent the mean ± SE of five animals for each group with each measurement performed in duplicate. A statistically significant increase (*, $P < 0.05$) was measured following PDT when compared to NT or to BO. NT: no treatment, BO: BPD only.

Figure 2

Analysis of tumor vasculature. The fluorescent molecule Alexa Fluor® 647-BSA was injected intravenously immediately before imaging the prostate tumor with the Maestro *in vivo* imaging system. Diffusion of the fluorescent molecule was imaged every 1 min for the first 10 min and every 2 min thereafter for a total imaging time of 20 min. Top graphs show the relative fluorescence measurements in the tumor as a function of time. Data was acquired from each boxed area. Bottom pictures are representative black and white (left) or fluorescent pictures (right) from untreated animals 21 days following implantation (A), 24 h post-treatment 22 days following implantation (B), and 96 h post treatment 24 days following implantation (C). Pictures were taken 20 min following fluorophore injection. Line: tumor borders. Box: area used for fluorescence measurements. Representative pictures are shown.

Figure 3

Treatment protocols. Orthotopic implantation of LNCaP cells in the prostate was done on day 1 and all animals were sacrificed on day 40. (A) Absolute control (n = 5). (B) PDT alone (n = 7).

(C) TNP-470 alone (n = 5). (D) TNP-470 treatment preceding PDT (n = 8), (E) PDT followed by TNP-470 treatment (n = 5). TNP-470 was injected at 30 mg/kg body weight every 2 days for 1 week. PDT was done with 0.25 mg/kg liposomal BPD injected 1 h prior to light irradiation (100 J/cm^2). N = number of animals in each groups.

Figure 4

Combination treatment improves local tumor control and reduces metastases. (A) Animals from each group were euthanized 40 days following tumor cell implantation. The prostate, comprised of both normal and tumor tissue, was weighed. There is a significant decrease (*, $P < 0.05$) in prostate weight in the PDT + TNP-470 group only when compared to the control. (B) At the time of sacrifice lymph nodes were collected, fixed in 10 % formalin, and embedded in paraffin. Sections were cut throughout the lymph node and assessed for metastases. N = number of animals in each groups.

Figure 5

Metastatic nodule in lymph node. Representative picture of microsection from formalin-fixed lymph nodes that was stained with hematoxylin and eosin. Metastatic spread was histologically determined. T: Metastatic nodule. N: normal lymph node.

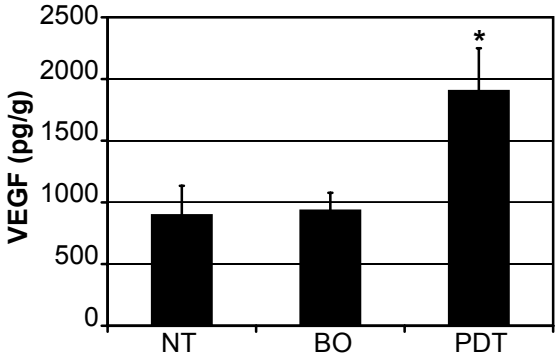

Figure 1

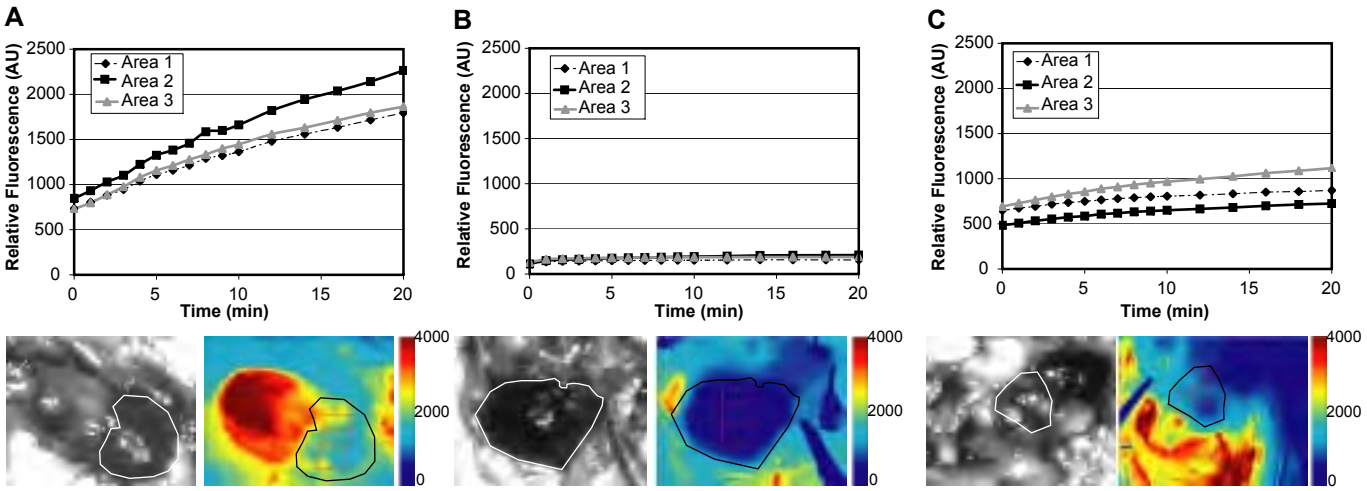
A
B
C
Relative Fluorescence (AU)
Time (min)
Area 1
Area 2
Area 3
0
500
1000
1500
2000
2500
0
5
10
15
20
4000
2000
0

Figure 2

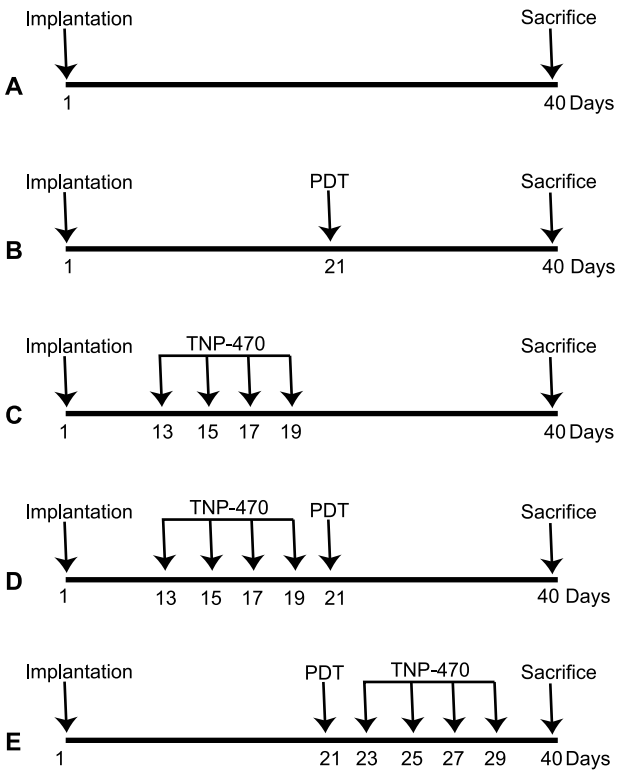
Implantation
Sacrifice
A
1
40 Days
Implantation
PDT
Sacrifice
B
1
21
40 Days
Implantation
TNP-470
Sacrifice
C
1
13
15
17
19
40 Days
Implantation
TNP-470
PDT
Sacrifice
D
1
13
15
17
19
21
40 Days
Implantation
PDT
TNP-470
Sacrifice
E
1
21
23
25
27
29
40 Days

Figure 3

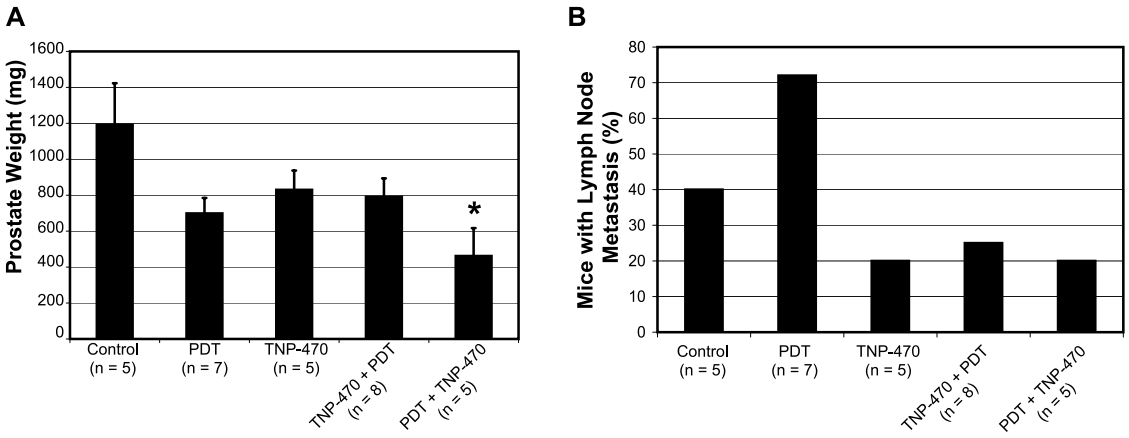
A
Prostate Weight (mg)
1600
1400
1200
1000
800
600
400
200
0
*
Control (n = 5)
PDT (n = 7)
TNP-470 (n = 5)
TNP-470 + PDT (n = 8)
PDT + TNP-470 (n = 5)
B
Mice with Lymph Node Metastasis (%)
80
70
60
50
40
30
20
10
0
Control (n = 5)
PDT (n = 7)
TNP-470 (n = 5)
TNP-470 + PDT (n = 8)
PDT + TNP-470 (n = 5)

Figure 4

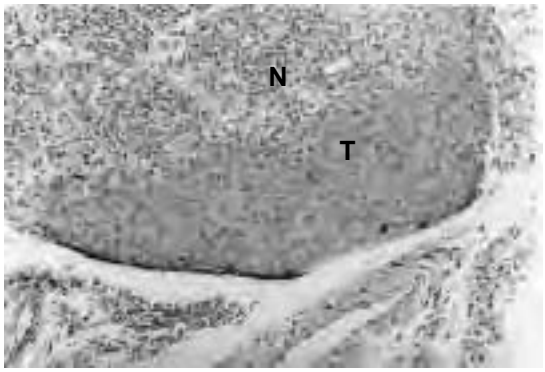

Figure 5

Decreased Cellular Adhesion Following Photodynamic Therapy of Prostate Cancer.

Nicolas Solban [1], Irene Georgakoudi [2], Sung K Chang[1], William L Rice[2], Charles Lin[1], Tayyaba Hasan [1,*].

[1]Wellman Center for Photomedicine, Massachusetts General Hospital, Harvard Medical School, Boston, Massachusetts. [2]Department of Biomedical Engineering, Tufts University, Medford, Massachusetts.

Running Title: PDT decreases adhesion of tumor cells to ECM

Key words: integrin, PDT, collagen, metastasis.

[*]Request for reprints: Tayyaba Hasan, Wellman Center for Photomedicine, Massachusetts General Hospital, 40 Blossom Street, Boston MA, 02114, Phone 617-726-6996; fax: 617-726-8566; E-mail: thasan@partners.org.

Acknowledgments

Grant support was provided by the National Institutes of Health Grant P01 CA84203 and R01 EB00664, and by the Department of Defense Grant PC040158 to N.S. during the preparation of this manuscript. We would like to thank QLT Inc. for the gift of BPD and liposomal BPD, E. Davis for editorial help, and Dr. Y. Chang for statistical analysis.

Abbreviations.

AIPC: androgen-independent prostate cancer.

ADPC: androgen dependent prostate cancer.

MLL: MatLyLu

BPD: Benzoporphyrin Derivative Monoacid Ring A.

LBPD: Lyposomal Benzoporphyrin Derivative Monoacid Ring A

PDT: Photodynamic Therapy.

ECM: extracellular matrix.

VEGF: vascular endothelial growth factor.

PS: Photosensitizer.

IVFC: *In vivo* Flow Cytometry.

Abstract

Adhesion molecules are essential for normal functioning of all organisms, by allowing communication between cells and the surrounding environment. For metastasis to occur a loss or a shift in expression pattern of adhesion molecules is often necessary. Furthermore, anticancer therapies have been reported to affect adhesion molecules. The current study investigates the effect of photodynamic therapy (PDT), an approved anticancer therapy, on prostate cancer cell adhesion and metastasis. Using the MatLyLu (MLL) cell line, a highly aggressive androgen-independent rat prostate cancer cell lines, we report that subcurative PDT transiently decreases adhesion to the extracellular matrix protein collagen IV. Furthermore, a transient decrease in β1 integrin protein levels but not of α5 integrin proteins was observed following PDT *in vitro*. RNA analysis did not show any decrease in β1 integrin or in α5 integrin levels, suggesting a post-translational effect of PDT on β1 integrin *in vitro*. Immunohistochemical, western and RT-PCR analysis of PDT treated orthotopic prostate tumors also showed a decrease in β1 integrin but not of α5 integrin. Next, we evaluated the effect of PDT on the circulation kinetics of prostate cancer cells by injecting cells in animals at various time post treatment and monitoring their circulation time using an *in vivo* flow cytometer (IVFC). 24 h after treatment, injected cells circulate longer than untreated cells while circulation time of cells injected 72 h after treatment were similar to untreated controls. The findings reported in this study shows that subcurative PDT transiently decreases adhesion of cells to extracellular matrix proteins as well as transiently increasing their circulation time. This understanding will greatly help in the design of novel mechanism-based combination treatment regimens.

Introduction

In tissue, cells are in constant communication with each other and with the surrounding environment. Adhesion molecules are essential for normal functioning of all organisms, by allowing these communications to take place. Adhesion molecules refer to all proteins that enable cells to contact and interact with each other or to interact with the extracellular matrix (ECM) (1). These include selectins, integrins, Ig superfamily, and cadherins. Integrins are a family of cell surface receptors that mediate interactions with ECM components. They are heterodimers composed of two subunits, α and β, and each αβ combination has its own binding specificity and signaling properties. As of now there are 8 β subunits that can assort with 18 α subunits to form 24 distinct integrins heterodimers and most of these heterodimers can recognize several ECM proteins (2). Alterations in adhesion molecules can be associated with pathological conditions: numerous evidence suggests that these molecules are associated with invasion and metastasis (3). For example, for metastasis to occur tumor cells must enter the blood or lymphatic circulation. This involves the loss of intercellular adhesion as well as the loss of adhesion to the ECM (4). Furthermore, during metastasis, cancer cells experience changing tissue microenvironments, which are likely to present novel matrix components. Therefore successful colonization often requires a shift in integrin expression and substrate preference.

Some anticancer therapies have been shown to decrease adhesion of cancer cells to ECM proteins. Fractionated ionizing radiation of prostate cancer cells has been shown to decrease the adhesion of prostate cancer cells to fibronectin, an ECM protein, as well as decreasing the expression of β1 integrin (5). The tyrosine kinase inhibitors, genistein and tyrphostin AG-1478, were also shown to decrease the adhesion of prostate cancer cells to collagen type I and type IV, laminin, fibronectin and vitronectin as well as decreasing the expression of β1 integrin (6). In

this report we investigated the effect of photodynamic therapy (PDT), an approved anticancer therapy, on the adhesion of prostate cancer cells to ECM. An understanding of the effect would help in the design of novel combination-based therapies.

PDT involves the delivery of a photosensitizer (PS), and its subsequent activation with the appropriate wavelength of light. For most non-dermatologic applications the PS is administered systemically in liposomal formulation and tends to accumulate non-specifically in tumor tissue because of its leaky vasculature, poor lymphatic drainage, and by binding to collagen or to LDL receptors highly expressed in tumors. Once activated the PS can 1) transfer its energy to O_2 generating the highly toxic, but short-lived singlet oxygen or 2) induce direct cell damage (7). The mode of tumor destruction depends on the localization of the PS at the time of treatment. When most of the PS is in circulation the predominant mode of tumor destruction is vascular shutdown, efficiently starving the tumor (8). On the other hand, when the PS is intratumoral, treatment will induce direct tumor destruction (9).

Over the last decade PDT became an established treatment modality for oncologic and non-oncologic conditions. Perhaps the best-known application of PDT is treatment of age-related macular degeneration with the PS verteporfin®. Approved oncologic applications for PDT include treatment of recurrent superficial papillary bladder cancer, esophageal cancer, endobronchial cancer, high-grade dysplasia associated with Barrett'oesophagus and as a palliative treatment for head and neck cancer. Currently, the use of PDT for localized disease and precancerous lesions is under investigation for bladder cancer, pituitary tumors, glioblastoma, and recurrent prostate cancer (10-13).

As PDT becomes more of a mainstream treatment option for early cancers, it is important to understand factors that might mitigate its tumoricidal effect. We have previously reported an

increase in the number of lung metastases following subcurative BPD-PDT in a highly aggressive prostate cancer model (14). Furthermore, in recent studies we showed that subcurative treatment of the human prostate cancer cell line, LNCaP, induces VEGF synthesis and release both *in vitro* and in an *in vivo* orthotopic model of prostate cancer (15). We also reported an increase in the incidence of lymph node metastases following subcurative PDT. This increase was abolished when an antiangiogenic molecule was administered after PDT (manuscript in preparation). Taken together these observations suggest that the tumor response to subcurative PDT may induce conditions favorable to metastatic spread or to tumor regrowth. An understanding of the tumor response will be useful in the development of molecular-based combination therapy to improve PDT. In the present study we investigated the effect of subcurative PDT on cell adhesion, an important step in the metastasic process.

To our knowledge only a few reports studied the effect of BPD-PDT on cell adhesion to the ECM (16, 17). In the current study we investigated the effect of subcurative BPD-PDT on cell-ECM adhesion *in vitro* and *in vivo* in an orthotopic model of prostate cancer using the androgen-independent, highly metastatic cell line, MLL. Our results indicate that subcurative treatment transiently reduces adhesion to collagen IV an abundant ECM protein and decreases β1 integrin protein levels both *in vitro* and *in vivo* without affecting α5 integrin levels. PDT also decreases β1 integrin mRNA levels *in vivo*. Furthermore, the circulation kinetics of injected PDT treated cells is transiently increased when compared to untreated controls. This increase in circulation time could provide a therapeutic opportunity to prevent re-adhesion of circulating cells and as a consequence decrease metastasis, this hypothesis merits further investigation.

Materials and Methods

Cell line and reagents

The rat prostate carcinoma cell line, MatLyLu was cultured as described previously (14). All cells were kept at 37^{o}C in a humidified 5% CO_2 and 95% air incubator. BPD-MA and LBPD were donated by QLT PhotoTherapeutics, Inc, (Vancouver, British Columbia, Canada). A concentration of 140 nM was used for *in vitro* assays and a concentration of 0.25 mg/kg body weight was used *in vivo*.

PDT

For *in vitro* PDT, $0.1x10^6$ of MLL cells were grown on a 35 mm culture dish for 24 h and incubated with BPD-MA [140 nM] in 1 ml complete media for 1 h. Incubation media was replaced with 2 ml of fresh complete media. Irradiation was performed using a 690 nm diode laser (High Power Devices, Inc., North Brunswick, NJ). 24 h following irradiation, cells viability was measured using the MTT assay (18). For *in vivo* PDT, LBPD was injected in the tail vein of rats 1 h prior to irradiation. Immediately before irradiation a laparotomy was performed and the prostate tumor was exposed. Tumors were irradiated at a fluence of 50 J/cm^2 with a fluence rate of 50 mW/cm^2. The incision is then closed and 24 h after treatment the animals are euthanized and the tumors are collected.

Tumor Implantation

Experiments were carried out on 8-weeks-old male Copenhagen rats weighing 200~ 250 g (Charles River Laboratories, Wilmington, MA). Animals were anesthetized with a 7:1 mixture of ketamine:xylazine. After anesthesia, a 2-cm longitudinal incision from the pubic bone in a cranial direction exposed the prostate after the bladder was retracted cranially. MLL cells were resuspended in PBS at a concentration 5 x 10^5/ml. A total of 0.1 ml (0.5 x 10^5 MLL cells) was

injected into the stroma of the prostate ventral lobe. The incision was closed with 2-0 suture, 7 days following injection a 125~150 mm^3 tumor develops.

RNA extraction and real-time RT-PCR analysis.
Total RNA was extracted from untreated or PDT treated MLL cells, using the Qiagen RNeasy mini kit (Qiagen Inc, Valencia, CA) according to the manufacturer's instruction. Possible genomic DNA contamination was removed by RNase-free DnaseI treatment (Qiagen Inc.). RNA concentration was estimated by reading the absorbance at 260 nm and RNA integrity was demonstrated by 1% agarose gel electrophoresis. First-strand cDNA was synthesized from 2 μg of RNA using Ready-To-Go You-Prime First-Strand Beads (Amersham Biosciences Corp, Piscataway, NJ) and Oligo(dT)15 Primer (Promega, Wisconsin, USA) according to the manufacturer's instructions and at the end of synthesis H2O was added up to 500 μl. For real time PCR analysis 5 μl of first strand cDNA product was amplified using Brilliant SYBR Green QPCR Master Mix (Stratagene, La Jolla, CA) according to the manufacturer's instructions in a total reaction volume of 25 μl using the following primers: GAPDH: forward 5'-ACT CCC ATT CTT CCA CCT TTG-3' and the reverse 5'-CAC CAC CCT GTT GCT GTA G-3', and α5 integrin: forward 5'–GGC TGT GTA TGG GGA GAA GA-3' and the reverse 5'–TCA CCG CGA AGT AGT CAC AG-3', and β1 integrin: forward 5'-GCG ATC AGG AGA ACC ACA G-3' and the reverse 5'-AAG CCA ATG CGG AAG TCT G-3'. The following conditions were used: 95^{o}C for 10 min, followed by 40 cycles of amplification (94^{o}C for 20 sec, 58^{o}C for 40 sec, 72^{o}C for 20 sec). The relative quantification of β1 integrin and α5 integrin was performed using the comparative C_T method using GAPDH as an endogenous reference. The following formula was used: $2^{-\Delta\Delta C_T}$. Where $\Delta\Delta C_T = \Delta C_T$ light only treatment - ΔC_T treatment.

Western blotting

Proteins were extracted from orthotopic prostate tumors or from MLL cells. Briefly, frozen tumors were pulverized to powder in tissue homogenizer and thawed in 1 ml/mg lysis buffer containing protease inhibitors (1% PBS, 1% Nonidet P-40, 0.5% sodium deoxycholate, 0.1% SDS, 10 mg/ml PMSF, 100 mM sodium orthovanadate, and protease inhibitors cocktail). MLL cells were resuspended directly in lysis buffer. Incubated on ice for 30 min with vortexing every 5 min then centrifuged 14 000 rpm for 10 min at 4^{o}C. The supernatant was transferred and centrifuged again. Protein concentration was determined using a standard Lowry method. Equal amount of proteins were separated by SDS-PAGE, blotted on PVDF membrane and probed with β1 integrin Ab (#610467, BD Biosciences, San Jose, CA), α5 integrin Ab (#sc-10729, Santa Cruz Biotechnology, Inc. Santa Cruz, CA) and monoclonal anti-Actin (#A-4700, Sigma-Aldrich, Saint-Louis, Mi).

Adhesion assay

At indicated times following PDT, $0.1x10^{6}$ MLL cells were collected and labeled with Vybrant DiO cell-labeling solution (Invitrogen, Carlsbad, CA) according to the manufacturer's instructions. Labeled cells were added to Collagen IV coated 24-well plate (Becton Dickinson Labware, Bedford, MA), and left to adhere for 6 h. Cells were then gently washed 4x with complete media, to remove unbound cells. % adhesion was calculated by taking the ratio of fluorescent counts after washes: fluorescent counts before washes.

In vivo flow cytometry

The experimental set-up for acquiring IVFC measurements has been described in detail in (19). To assess the depletion kinetics of circulating PDT-treated MLL cells, MLL cells were labeled

with the lipophilic dye, DiD, according to the manufacturer's instruction (Invitrogen, Carlsbad, CA). 10^6 fluorescently labeled cells per 20 g body weight were injected through the tail vein of a male SCID mouse; the animal was placed immediately onto the stage. The first IVFC measurements were acquired within five to fifteen minutes from the time of injection. Additional measurements were acquired at the same vessel location at 1, 2, and 3 h.

Immunohistochemistry.

PDT treated tumors were fixed in 10% formalin and embedded in paraffin. Tissue sections were deparaffinized and subjected to heat induced epitope retrieval. Sections were then immersed 30 min in 0.3% H_2O_2 to quench endogenous peroxidase activity, then blocked with normal mouse serum for 20 min (Vectastain ABC kit, Vector Laboratories, Burlingame, CA). Sections were then incubated overnight at 4^oC with β1 integrin Ab at a dilution of 1:50, washed and incubated with biotinylated secondary Ab for 30 min. Slides were then incubated with avidin-peroxidase conjugate for 30 min. After washing, sections are stained with DAB (DakoCytomation, Carpinteria, CA) for 3 min.

Results

Sublethal PDT transiently decreases adhesion to collagen IV. After 1 hr incubation with BPD-MA, MLL cells were irradiated with a 690 nm laser at different light doses. Figure 1 shows MLL killing as a function of light doses. These cells are highly susceptible to PDT killing, the very low light dose, 0.25 J/cm^2 kills approximately 15% of cells while 1.5 J/cm^2 kills about 80% of cells. In order to study the molecular response of cells that have been exposed to both PS and PDT but not enough to kill them we have chosen the two subcurative doses, 0.5 J/cm^2 and 1 J/cm^2 for all subsequent experiments. These doses kill approximately 30% and 70% of cells respectively (Figure 1, grey bars). To determine the effect of subcurative PDT on cell adhesion we plated cells 24 h and 72 h following subcurative PDT, on collagen IV coated plates. PDT treatment with the higher light dose reduced adhesion to collagen IV more than 5-fold, 24 h following treatment (Figure 2, A). Lower light dose treatment did not have any effect on adhesion to collagen IV. Interestingly, 72 h following treatment adhesion to collagen IV is returned to control level (Figure 2, B). To evaluate the effect of cell detachment on cell survival we plated MLL cells on 1%-agar/RPMI. This formulation has been shown to prevent cell adhesion and induce cell death (20). 24 h and 48 h later the trypan exclusion assay was used to quantify cell survival. MLL cells are highly resistant to anoikis with only 4.92% ± 1.62 and 5.96% ± 1.88 of cells dying 24 h and 48 h respectively, after plating.

Subcurative PDT transiently decreases β1 integrin protein levels. The α5β1 integrin is highly expressed in MLL cells (21, 22) and mediates adhesion to collagen IV. We therefore, evaluated the levels of α5 and β1 integrin following PDT. Figure 3 shows representative western blot detecting β1 integrin and α5 integrin, together with actin as a loading control. PDT treatment

with the higher light dose transiently decreases β1 integrin protein levels (Figure 3, A), 24 h after treatment. β1 integrin levels return to control levels 72 h after PDT Figure 3, B. Surprisingly, α5 integrin levels were not decreased following PDT. To elucidate the mechanism of this decrease, we measured RNA levels following treatment. Real-time PCR analysis did not show any decrease in mRNA transcript of either α5 integrin or β1 integrin (Figure 3, C and D respectively), suggesting a post-translational effect of PDT.

In vivo decrease in β1 integrin following subcurative PDT. Orthotopic implantation of MLL cells is a well-established model of androgen-independent prostate cancer. This cell line is fast growing, poorly differentiated, and metastatic to the lungs and lymph nodes. To determine if this subcurative PDT-induced decrease in β1 integrin also occurred *in vivo*, we implanted MLL cells in the prostate of Copenhagen rats and treated them with 50 J/cm^2. The PDT regimen used has previously been demonstrated to be subcurative (23). Twenty-four hours following treatment, animals were euthanized and the prostate was collected and fixed in 10 % formalin. Figure 4 show immunohistochemical staining using β1 integrin Ab. Similar to *in vitro* results; there is a decrease in β1 integrin protein levels following PDT treatment. Figure 4, right panels, arrow, shows an area unaffected by PDT treatment. This area probably did not receive enough light or PS, or both to elicit visible damage. Proteins were also extracted from PDT treated tumors and western blot analysis was performed to determine the levels of α5 and β1 integrin. There is a significant decrease in β1 protein levels (Figure 5, left picture) following PDT, however there is no decrease in α5 integrin protein levels (Figure 5, right picture). The average densitometric quantification from 5 different animals is presented in the lower bar graph after taking the ratio integrin: actin. Following PDT there is a 5-fold decrease in β1 integrin protein levels (Figure 5,

left bar graph); but no significant decrease in α5 integrin protein levels. From the same PDT-treated tumors RNA was extracted, there is a significant decrease in β1 integrin mRNA levels following treatment ($P < 0.001$ when compared to no treatment) and, surprisingly, a significant increase in α5 integrin mRNA ($P < 0.05$ when compared to no treatment, Figure 5, C and D).

Subcurative PDT increases circulation time of MLL cells. Adhesion molecules are required for homing of circulating cancer cells and subcurative PDT-treatment decreases adhesion to collagen IV. Therefore, we evaluated the effect of subcurative PDT on the circulation time of MLL cells. PDT-treated or untreated MLL cells were labeled with the lipophilic fluorescent dye, DiD, prior to intravenous injection in animals. Live, anesthetized animals were placed on the IVFC to count circulating cells (24). Untreated cells are very rapidly cleared from circulation, 30 min after injection, there is a ~ 80 % decrease in the number of circulating cells (Figure 6, gray plot). However, when cells are injected 24 h following PDT, there is a significant ($P < 0.05$ when compared to control) increase in circulation time (Figure 6, dash plot), while cells injected 72 h post-PDT have similar circulation time than control (Figure 6, black plot).

Discussion

It is important to understand factors that limit anticancer therapies in order to improve treatment outcome. Recently, the concept of PDT-elicited tumor survival response has emerged, whereas surviving tumor cells secrete cytokines that promote tumor regrowth and, potentially, metastasis (15, 25, 26). We and others have reported an increase in VEGF following subcurative PDT (15, 25, 27, 28), suggesting that surviving, PDT-treated cells, elicit a survival response that could be detrimental to long term cure. Furthermore, we have reported that subcurative PDT of prostate cancer increased the incidence of lymph node metastasis and that combination treatment with an antiangiogenic molecule not only decreased the incidence of lymph node metastasis but also improved local control, demonstrating that rationally designed mechanism-based combination therapies will improve treatment outcome (manuscript in preparation). However, it is well established that metastasis involves an intricate interplay between angiogenesis/lymphangiogenesis, altered cell adhesion, survival, proteolysis, migration, immune escape, and homing on target organs. Therefore, VEGF may not be the only player responsible for the observed increased in metastasis. In the current study we investigated the effect of PDT on prostate cancer cell adhesion to ECM, another process often altered during metastasis.

Due to the limited penetration depth of light in tissue and to the non-homogeneous distribution of the PS inside the tumor, some areas will receive suboptimal PDT (either not enough light or not enough PS, or both), especially when treating large tumor volumes. This can be observed in Figure 4, where the arrow points to an area unaffected by treatment. Surviving PDT-treated cells elicit a survival response that includes the secretion of growth factors (15, 29) and, as reported in this study, a decrease in adhesion. These molecular changes could mitigate treatment efficacy by promoting tumor regrowth or increasing metastasis unless combined with

other therapy (manuscript in preparation). Furthermore taken together, these results also illustrate the need for better dosimetry of PS and light in tissue in order to improve treatment (30).

In a previous study, Margaron et al., reported a decrease in adhesion to ECM proteins following BPT-PDT of human foreskin fibroblast, however they did not observe a decrease in integrins protein levels. On the other hand, they reported a decrease in phosphorylation of the Focal Adhesion Kinase following PDT (17). We have also previously reported that subcurative BPD-PDT of a human ovarian cancer cell line decreased adhesion to ECM proteins (16) without affecting integrins levels, but by disrupting focal adhesion plaques. We report in this study, using a highly aggressive prostate cancer cell line that PDT transiently decreased adhesion to the ECM protein collagen IV as well as transiently decreasing β1 integrin protein levels. Taken together these reports suggest that the response to PDT may be cell type dependent. Of note, the observed decrease in adhesion to ECM is not unique to PDT but has also been reported to occur following ionizing radiation and tyrosine kinase inhibitor treatment (5, 6) of prostate cancer cells.

We have shown that subcurative PDT transiently decreases adhesion to collagen IV an abundant ECM protein and reduces β1 integrin protein levels both in vitro and in vivo. β1 integrin mRNA analysis did not show any difference in vitro, however, protein levels were decreased. A report by Volanti et al., showed that PDT could disrupted the membrane expression of ICAM-1 and VCAM-1 via their degradation in lysosomes (31). It is possible that, in vitro, β1 integrin is degraded via a similar pathway or by other mechanisms (32). In vivo, on the other hand, mRNA levels are also decreased suggesting an effect of PDT on β1 integrin promoter activity. In vitro, α5 integrin mRNA levels were not increased by PDT, on the other hand its levels were increased in vivo. A recent report showed that the α5 integrin promoter was activated by the hypoxia-inducible factor (HIF-1α (33)). Since it is well established that PDT

generates hypoxic conditions in vivo (34-36), PDT could increase α5 integrin mRNA in vivo through a HIF-1α mechanism. On the other hand, we have never observed activation of HIF-1α in vitro following PDT (15).

Previous reports have shown that the α5β1 integrin molecule is important for cancer cell invasion (21) and adhesion (37). In this study we report a decrease in β1 integrin post-PDT; however we did not measure a resulting decrease in invasion (invasion assay, data not shown). This is not surprising since MLL cells are highly aggressive and invasive (38). A consequence of a decrease in adhesion is the activation of anoikis (39), we did not measure any increase in cell death when adhesion was blocked. From the data presented in this study as well as from previous reports ((15) and manuscript in preparation) we propose a model for PDT-elicited tumor survival response that can be detrimental to long term health unless combined with other treatment regimens. Subcurative PDT increases the release of VEGF, we have measured a 2.3 fold increase in VEGF mRNA (data not shown), and a decrease in adhesion. Combined, this increases the release of cancer cells and potentially leads to metastases. Released cells will have longer circulation time, due to the PDT-induced decrease in adhesion molecules, therefore creating a window of opportunity to prevent their adhesion to metastatic sites.

The relevance of the current study concerns suboptimal PDT, with our investigation of the biological response of tumor cells that have received sublethal PDT. Our focus is on factors that might impede treatment efficacy. We and others have previously reported and increase in VEGF following subcurative PDT treatment (15) that could promote tumor regrowth (29) and metastasis (manuscript in preparation). However, other factors may also play a detrimental role depending on the tumor type or stage of the disease. For these reasons we have chosen the highly aggressive, androgen-independent MLL prostate cancer cell line for this study. This cell line is

useful for studying AIPC, which occurs at a later stage in prostate cancer. This study shows that sublethal and subcurative PDT transiently decreases the expression of adhesion molecules as well as transiently increasing the *in vivo* circulation time of PDT treated cells. Furthermore, the results presented in this study suggest a possible mechanism for the previously described increase in metastasis following subcurative PDT of MLL tumors (14) and provide the rational for the development of combination therapy for improving PDT.

References

1. Chothia C, Jones EY. The molecular structure of cell adhesion molecules. Annu Rev Biochem. 1997;66:823-62.

2. Arnaout MA, Mahalingam B, Xiong JP. Integrin structure, allostery, and bidirectional signaling. Annu Rev Cell Dev Biol. 2005;21:381-410.

3. Chin D, Boyle GM, Kane AJ, et al. Invasion and metastasis markers in cancers. Br J Plast Surg. 2005; Jun;58:466-74.

4. Bogenrieder T, Herlyn M. Axis of evil: Molecular mechanisms of cancer metastasis. Oncogene. 2003; Sep 29;22:6524-36.

5. Simon EL, Goel HL, Teider N, Wang T, Languino LR, Fitzgerald TJ. High dose fractionated ionizing radiation inhibits prostate cancer cell adhesion and beta(1) integrin expression. Prostate. 2005; Jun 15;64:83-91.

6. Skogseth H, Holt RU, Larsson E, Halgunset J. Tyrosine kinase inhibitors alter adhesivity of prostatic cancer cells to extracellular matrix components. APMIS. 2006; Mar;114:225-33.

7. Hasan T, Ortel B, Solban N, Pogue B. Photodynamic therapy of cancer. In: Kufe, Bast, Hait, Hong, Pollock, Weichselbaum, et al, editors. Cancer Medicine, 7th edition. Hamilton, Ontario: B.C. Decker, Inc; 2006. p. 537-548.

8. Wang HW, Putt ME, Emanuele MJ, et al. Treatment-induced changes in tumor oxygenation predict photodynamic therapy outcome. Cancer Res. 2004; Oct 15;64:7553-61.

9. Ahmad N, Mukhtar H. Mechanism of photodynamic therapy-induced cell death. Methods Enzymol. 2000;319:342-58.

10. Dougherty TJ. An update on photodynamic therapy applications. J Clin Laser Med Surg. 2002; Feb;20:3-7.

11. Brown SB, Brown EA, Walker I. The present and future role of photodynamic therapy in cancer treatment. Lancet Oncol. 2004; Aug;5:497-508.

12. Windahl T, Andersson SO, Lofgren L. Photodynamic therapy of localised prostatic cancer. Lancet. 1990; Nov 3;336:1139.

13. Nathan TR, Whitelaw DE, Chang SC, et al. Photodynamic therapy for prostate cancer recurrence after radiotherapy: A phase I study. J Urol. 2002; Oct;168:1427-32.

14. Momma T, Hamblin MR, Wu HC, Hasan T. Photodynamic therapy of orthotopic prostate cancer with benzoporphyrin derivative: Local control and distant metastasis. Cancer Res. 1998; Dec 1;58:5425-31.

15. Solban N, Selbo PK, Sinha AK, Chang SK, Hasan T. Mechanistic investigation and implications of PDT-induction of VEGF in prostate cancer. Cancer Res. 2006; May 15;66:1-8.

16. Runnels JM, Chen N, Ortel B, Kato D, Hasan T. BPD-MA-mediated photosensitization in vitro and in vivo: Cellular adhesion and beta1 integrin expression in ovarian cancer cells. Br J Cancer. 1999;80:946-953.

17. Margaron P, Sorrenti R, Levy JG. Photodynamic therapy inhibits cell adhesion without altering integrin expression. Biochim Biophys Acta. 1997;1359:200-10.

18. Merlin JL, Azzi S, Lignon D, Ramacci C, Zeghari N, Guillemin F. MTT assays allow quick and reliable measurement of the response of human tumour cells to photodynamic therapy. Eur J Cancer. 1992;28A:1452-8.

19. Novak J, Georgakoudi I, Wei X, Prossin A, Lin CP. In vivo flow cytometer for real-time detection and quantification of circulating cells. Opt Lett. 2004; Jan 1;29:77-9.

20. Boisvert-Adamo K, Aplin AE. B-RAF and PI-3 kinase signaling protect melanoma cells from anoikis. Oncogene. 2006; Aug 10;25:4848-56.

21. Livant DL, Brabec RK, Pienta KJ, et al. Anti-invasive, antitumorigenic, and antimetastatic activities of the PHSCN sequence in prostate carcinoma. Cancer Res. 2000; Jan 15;60:309-20.

22. MacCalman CD, Brodt P, Doublet JD, et al. The loss of E-cadherin mRNA transcripts in rat prostatic tumors is accompanied by increased expression of mRNA transcripts encoding fibronectin and its receptor. Clin Exp Metastasis. 1994; Mar;12:101-7.

23. Momma T, Hamblin MR, Wu HC, Hasan T. Photodynamic therapy of orthotopic prostate cancer with benzoporphyrin derivative: Local control and distant metastasis. Cancer Res. 1998; Dec 1;58:5425-31.

24. Georgakoudi I, Solban N, Novak J, et al. In vivo flow cytometry: A new method for enumerating circulating cancer cells. Cancer Res. 2004; Aug 1;64:5044-7.

25. Ferrario A, von Tiehl KF, Rucker N, Schwarz MA, Gill PS, Gomer CJ. Antiangiogenic treatment enhances photodynamic therapy responsiveness in a mouse mammary carcinoma. Cancer Res. 2000; Aug 1;60:4066-9.

26. Ferrario A, Gomer CJ. Avastin enhances photodynamic therapy treatment of kaposi's sarcoma in a mouse tumor model. J Environ Pathol Toxicol Oncol. 2006;25:251-60.

27. Uehara M, Inokuchi T, Sano K, ZuoLin W. Expression of vascular endothelial growth factor in mouse tumours subjected to photodynamic therapy. Eur J Cancer. 2001; Nov;37:2111-5.

28. Jiang F, Zhang ZG, Katakowski M, et al. Angiogenesis induced by photodynamic therapy in normal rat brains. Photochem Photobiol. 2004; Jun;79:494-8.

29. Ferrario A, von Tiehl KF, Rucker N, Schwarz MA, Gill PS, Gomer CJ. Antiangiogenic treatment enhances photodynamic therapy responsiveness in a mouse mammary carcinoma. Cancer Res. 2000; Aug 1;60:4066-9.

30. Zhou X, Pogue BW, Chen B, et al. Pretreatment photosensitizer dosimetry reduces variation in tumor response. Int J Radiat Oncol Biol Phys. 2006; Mar 15;64:1211-20.

31. Volanti C, Gloire G, Vanderplasschen A, Jacobs N, Habraken Y, Piette J. Downregulation of ICAM-1 and VCAM-1 expression in endothelial cells treated by photodynamic therapy. Oncogene. 2004; Nov 11;23:8649-58.

32. Lee I, Skinner MA, Guo HB, Sujan A, Pierce M. Expression of the vacuolar H+-ATPase 16-kDa subunit results in the triton X-100-insoluble aggregation of beta1 integrin and reduction of its cell surface expression. J Biol Chem. 2004; Dec 17;279:53007-14.

33. Spangenberg C, Lausch EU, Trost TM, et al. ERBB2-mediated transcriptional up-regulation of the alpha5beta1 integrin fibronectin receptor promotes tumor cell survival under adverse conditions. Cancer Res. 2006; Apr 1;66:3715-25.

34. Sitnik TM, Hampton JA, Henderson BW. Reduction of tumour oxygenation during and after photodynamic therapy in vivo: Effects of fluence rate. Br J Cancer. 1998;77:1386-94.

35. Henderson BW, Busch TM, Vaughan LA, et al. Photofrin photodynamic therapy can significantly deplete or preserve oxygenation in human basal cell carcinomas during treatment, depending on fluence rate. Cancer Res. 2000; Feb 1;60:525-9.

36. Chen Q, Huang Z, Chen H, Shapiro H, Beckers J, Hetzel FW. Improvement of tumor response by manipulation of tumor oxygenation during photodynamic therapy. Photochem Photobiol. 2002; Aug;76:197-203.

37. Dalton SL, Marcantonio EE, Assoian RK. Cell attachment controls fibronectin and alpha 5 beta 1 integrin levels in fibroblasts. implications for anchorage-dependent and -independent growth. J Biol Chem. 1992; Apr 25;267:8186-91.

38. Isaacs JT, Isaacs WB, Feitz WF, Scheres J. Establishment and characterization of seven dunning rat prostatic cancer cell lines and their use in developing methods for predicting metastatic abilities of prostatic cancers. Prostate. 1986;9:261-81.

39. Frisch SM, Francis H. Disruption of epithelial cell-matrix interactions induces apoptosis. J Cell Biol. 1994; Feb;124:619-26.

Figure legend

Figure 1: Survival of MLL cells as a function of light dose. 24 h following PDT treatment with the indicated light doses, MTT assay was performed to determine cells survival. LO was arbitrarily set at 100 %. For subsequent experiments light doses of 0.5 J/cm^2 and 1 J/cm^2 were used (grey bars). LO: Light Only, BO: BPD Only. Results are mean ± SE of 3 independent experiments measured in duplicate.

Figure 2: Subcurative PDT decreases adhesion to Collagen IV. (A) 24 h or 72 h (B) post-PDT MLL cells were collected, labeled with DiO, plated on Collagen IV coated 24-well plate, and left to adhere for 6 h. Cells were then either washed 4x to remove unbound cells or left unwashed to measure total cells plated. % Adhesion was calculated by taking the fluorescent count of bound cells (after washing) to the fluorescent count of total cells plated (unwashed). LO: Light Only, BO: BPD Only. % = % of cells that survived treatment. Results are mean ± SE of 3 independent experiments.

Figure 3: In vitro analysis of β1 integrin and α5 integrin protein and mRNA levels. MLL cells were incubated with BPD-MA for 1 h before subcurative treatment. At 24 h (A) and 72 h (B) following treatment, cells were collected, protein extracted and 100 μg or 25 μg was used for β1 integrin and α5 integrin western respectively. The level of actin was measured as a protein-loading control. (C) Real-time RT-PCR analysis of α5 and β1 integrin mRNA levels. Results are expressed relative to LO and are mean ± SE of 3 independent experiments measured in triplicate. LO: Light Only, BO: BPD Only, % = % of cells that survived treatment.

Figure 4: Immunohistochemical staining of β1 integrin in orthotopic prostate tumors. Microsections of tumors were stained with hematoxylin and eosin (H & E, top pictures) or with β1 integrin and hematoxylin (bottom figures). Arrow indicates area unaffected by treatment. NT: No treatment, PDT represents two different tumors.

Figure 5: Analysis of β1 integrin and α5 integrin protein levels from orthotopic prostate tumors. 24 h following PDT, animals were sacrificed, tumors were collected and proteins and RNA were extracted. 100 μg or 25 μg of proteins was used for β1 integrin (A) and α5 integrin (B) western respectively. The level of actin was measured as a protein-loading control. PDT 1 and PDT 2 are proteins from tumors of 2 different animals. Graphs represent the average integrin β1 levels (left) or α5 levels (right) from 5 different tumors after calculating the integrin: actin ratio and performing densitometric analysis. Real-time RT-PCR analysis of β1 (C) and α5 (D) integrin mRNA levels. Results are expressed relative to NT and are mean ± SE of 5 independent experiments measured in triplicate. NT was arbitrarily set at 1. NT: No treatment, BO: BPD Only. ** $p < 0.001$, and * $p < 0.05$ when compared to NT.

Figure 6: Subcurative PDT increases circulation time of prostate cancer cells. 24 h (-▲-) or 72 h (-■-) post-PDT or untreated (-◊-) MLL were labeled with the lipophilic dye DiD and injected in the tail vein of SCID mice and immediately placed on the IVFC. The normalized numbers of circulating cells per minute are shown for 3 h following injection of the fluorescently labeled cells. (n=3 with 5 measurements). * $P < 0.05$ when compared to untreated cells.

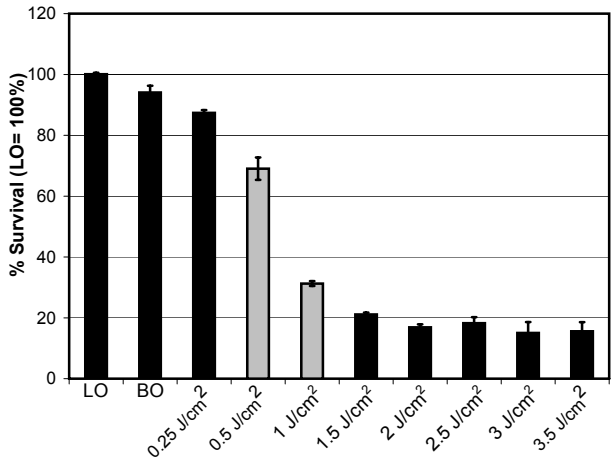
% Survival (LO= 100%)
120
100
80
60
40
20
0
LO
BO
0.25 J/cm2
0.5 J/cm2
1 J/cm2
1.5 J/cm2
2 J/cm2
2.5 J/cm2
3 J/cm2
3.5 J/cm2

Figure 1

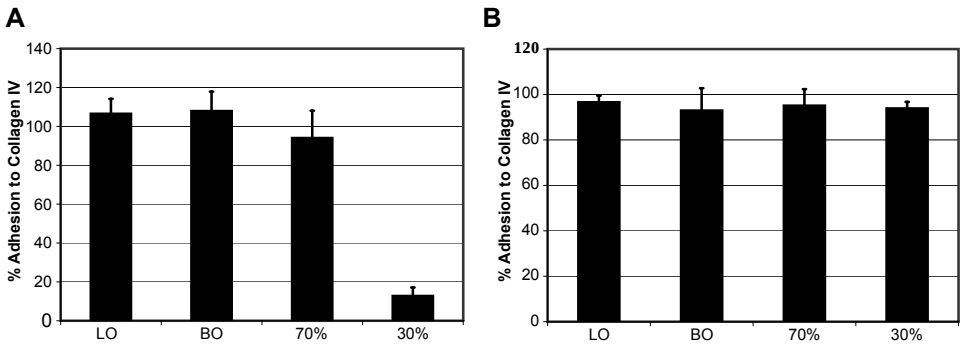
A
% Adhesion to Collagen IV
140
120
100
80
60
40
20
0
LO
BO
70%
30%
B
% Adhesion to Collagen IV
120
100
80
60
40
20
0
LO
BO
70%
30%

Figure 2

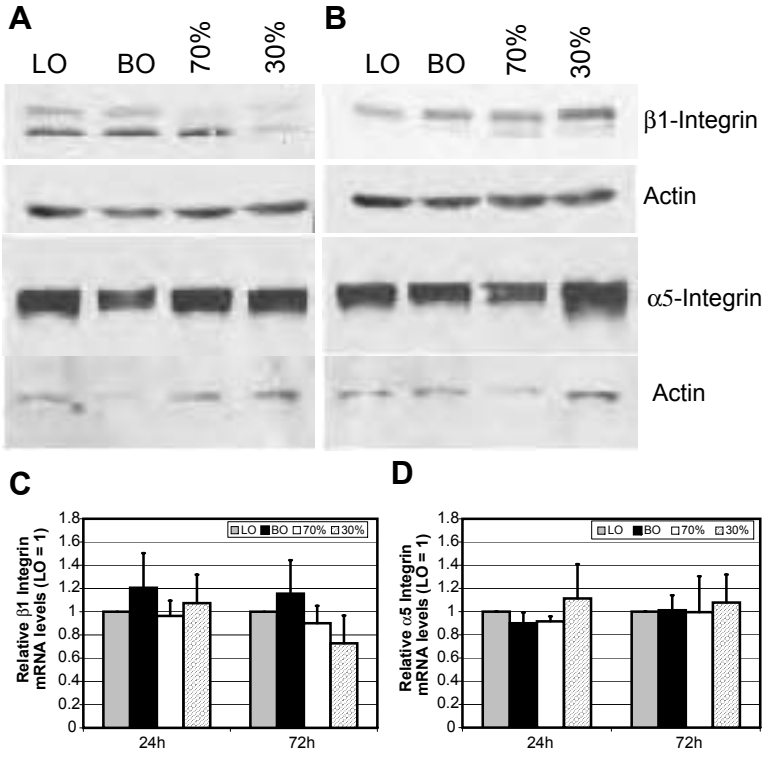
A
LO
BO
70%
30%
B
LO
BO
70%
30%
β1-Integrin
Actin
α5-Integrin
Actin
C
Relative β1 Integrin mRNA levels (LO = 1)
LO BO 70% 30%
1.8
1.6
1.4
1.2
1
0.8
0.6
0.4
0.2
0
24h
72h
D
Relative α5 Integrin mRNA levels (LO = 1)
LO BO 70% 30%
1.8
1.6
1.4
1.2
1
0.8
0.6
0.4
0.2
0
24h
72h

Figure 3

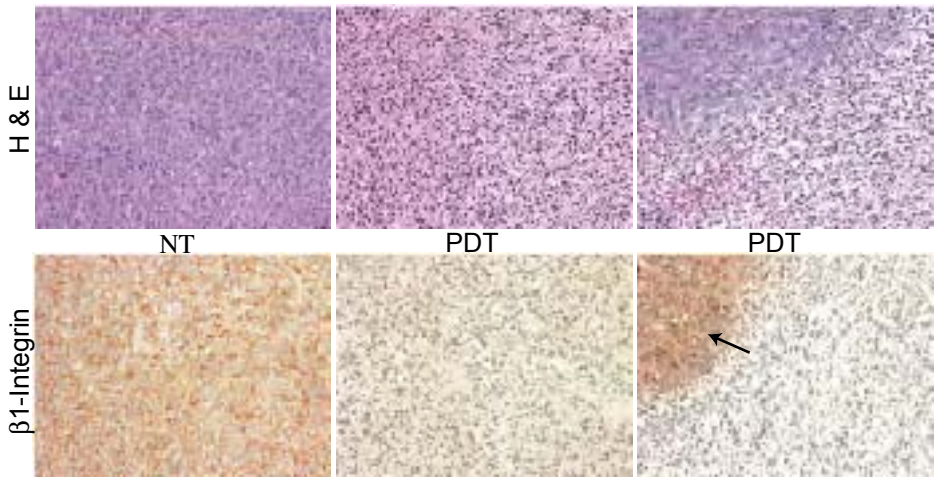

Figure 4

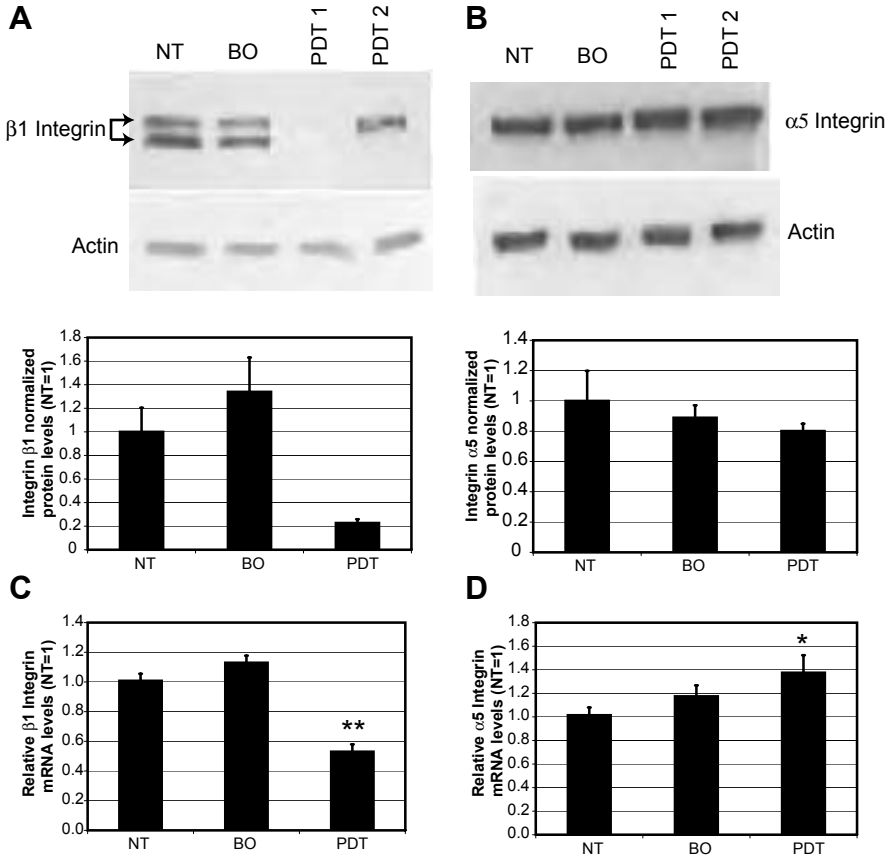
A
NT
BO
PDT 1
PDT 2
β1 Integrin
Actin
B
NT
BO
PDT 1
PDT 2
α5 Integrin
Actin
Integrin β1 normalized protein levels (NT=1)
1.8
1.6
1.4
1.2
1
0.8
0.6
0.4
0.2
0
NT
BO
PDT
Integrin α5 normalized protein levels (NT=1)
1.4
1.2
1
0.8
0.6
0.4
0.2
0
NT
BO
PDT
C
Relative β1 Integrin mRNA levels (NT=1)
1.4
1.2
1.0
0.8
0.6
0.4
0.2
0.0
**
NT
BO
PDT
D
Relative α5 Integrin mRNA levels (NT=1)
1.8
1.6
1.4
1.2
1.0
0.8
0.6
0.4
0.2
0.0
*
NT
BO
PDT

Figure 5

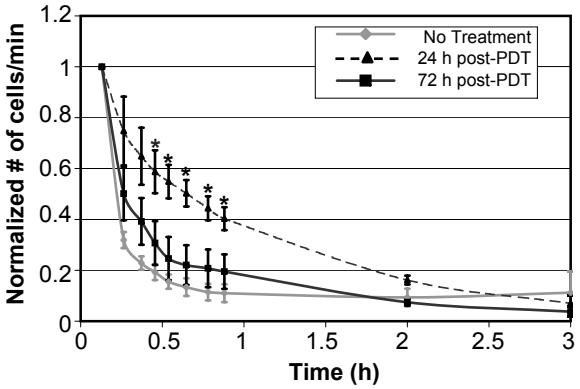
Normalized # of cells/min
Time (h)
No Treatment
24 h post-PDT
72 h post-PDT
1.2
1
0.8
0.6
0.4
0.2
0
0
0.5
1
1.5
2
2.5
3
*
*
*
*
*

Figure 6